Bulletin of the Seismological Society of America, Vol. 77, No. 3, pp. 784–808, June 1987

COMPARISON OF THE 1959 HEBGEN LAKE, MONTANA AND THE 1983 BORAH PEAK, IDAHO, EARTHQUAKES FROM GEODETIC OBSERVATIONS

BY SERGIO E. BARRIENTOS, ROSS S. STEIN, AND STEVEN N. WARD

ABSTRACT

We deduce the fault geometry, coseismic slip, and moment for two of the largest historic earthquakes that have occurred in the Basin and Range of the Western United States: the $M = 7.3$ 1959 Hebgen Lake, Montana, earthquake and the $M = 6.9$ 1983 Borah Peak, Idaho, event. Newly augmented data sets of vertical deformation from geodetic leveling and from lake shoreline changes were modeled by simple dislocations in an elastic half-space. The rms signal-to-noise ratio is 12 for the Hebgen Lake data and 38 for the Borah Peak set. The residuals for both models are about twice as large as the noise. The Hebgen Lake earthquake struck on the 15- to 25-km-long en-echelon Hebgen and Red Canyon faults, dipping 45° to 50° and extending to a depth of 10 to 15 km. The 7.0 and 7.8 m of dip-slip on these faults produced a combined moment of 1.2×10^{20} N-m. The dip of the Red Canyon fault may decrease slightly with depth (in a listric manner), abutting the planar Hebgen fault at a depth of 8 km. In addition, up to 1 m of deep slip occurred on the Holocene segment of the adjacent Madison Range fault, 10 km west of the Hebgen fault. The Borah Peak segment of the Lost River fault was found to dip 49°. Slip of 2.1 m occurred at the south fault end, extending to a depth of 14 km; 1.4 m of slip occurred at the north end, where the fault reached only to 6 km depth. A listric fault shape is not permitted by the geodetic data at Borah Peak. Both the Hebgen-Red Canyon and the Lost River faults are high-angle and nearly planar, despite the much greater age and length of the Lost River fault in comparison to the en-echelon Hebgen faults. The chief difference between the earthquakes is the 3- to 4-fold higher slip at Hebgen relative to Borah Peak and all other well-studied Basin and Range shocks. Thrust faults located close to these active normal faults must either dip steeply at depth or were not reactivated.

INTRODUCTION

The 1959 Hebgen Lake ($M = 7.3$) and the 1983 Borah Peak ($M = 6.9$) earthquakes are two of the largest normal faulting events to have occurred historically in the United States (Figure 1). The 1983 Borah Peak earthquake was well-recorded both seismically and geodetically. The 1959 Hebgen Lake event possesses a more complete geodetic record than a seismic record. In this study, we use measurements of the vertical deformation of the ground to deduce the subsurface geometry of the Hebgen Lake-Red Canyon fault in Montana and the Lost River fault in Idaho. We vary the fault dimensions, orientation, and the curvature of the fault with depth, and invert for the slip.

This comparison affords the chance to learn how the geometry of a youthful normal fault differs from an older normal fault. Since both faults are associated with older thrusts, we also test whether the normal faults flatten with depth as do other exhumed thrusts and some active normal faults (Wernicke, 1981; Allmendinger *et al.*, 1983) in the Basin and Range Province.

Leveling observations of the elevation changes associated with both earthquakes are augmented by new data. With the help of Gary Perasso, we recovered unpublished U.S. Geological Survey leveling records from the Hebgen Lake area for the

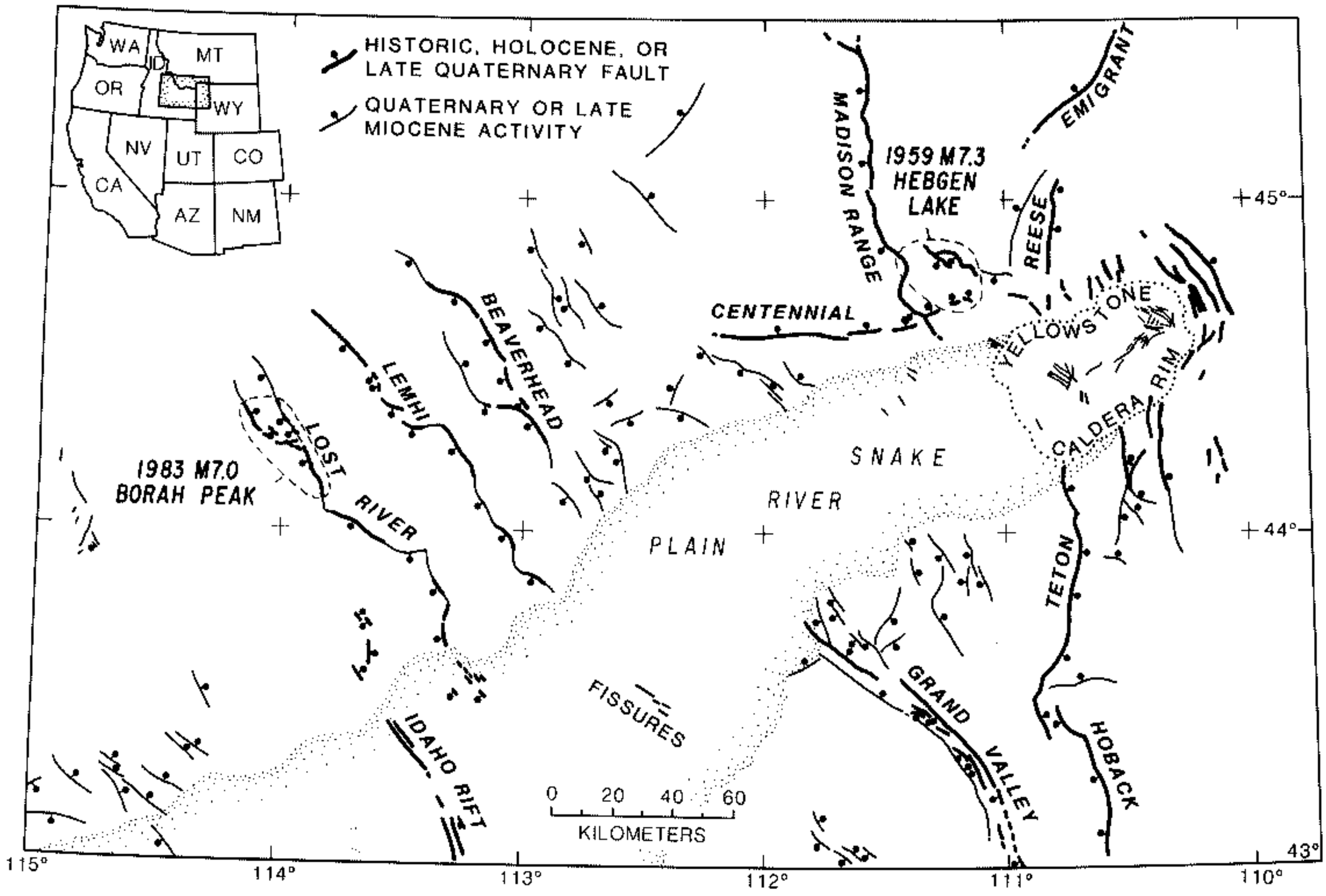

FIG. 1. Neotectonic setting of the 1983 Borah Peak and the 1959 Hebgen Lake earthquakes in the northeastern Basin and Range Province.

preseismic and postseismic periods. These new data consists of a 20-km-long segment that allow testing the data quality in a loop around the lake. The leveling data is supplemented by Myers and Hamilton's (1964) measurements of changes in the Hebgen Lake shore and leveling turning points on the highway (Figure 2). With these observations, we extend the work of Savage and Hastie (1966) on the Hebgen Lake earthquake to examine multiple en-echelon and curved faults. At Borah Peak in 1985, the National Geodetic Survey completed a new leveling survey oriented parallel to the Lost River fault. This line was previously leveled in 1933 (Figure 3). Barrientos *et al.* (1985), Stein and Barrientos (1985a, b), and Ward and Barrientos (1986) modeled the source parameters of the 1983 earthquake using only a fault-crossing leveling line oriented normal to the fault. The new line enhances the resolution of the fault geometry and slip along the central and northern portions of the rupture where antithetical faulting occurred.

Although both earthquakes resulted from crustal extension in the northern Basin and Range Province, the faults on which the shocks struck have different histories and shapes: the Lost River fault is considerably older, and 4 times longer, than the Hebgen Lake-Red Canyon fault. The Borah Peak earthquake ruptured the central 35-km segment of the 100-km-long Lost River fault (Figure 1). The fault has displaced formerly adjacent beds about 3 km vertically and has been active for the past 4 to 7 m.y. (Scott *et al.*, 1985). The Yellowstone hot spot (Smith and Christiansen, 1980) crossed the south end of the Lost River fault about 5 m.y. ago. The White Knob thrust fault, which was active during the Laramide Orogeny, strikes parallel to and lies 2 to 5 km basinward of the Lost River normal fault (Bond, 1978).

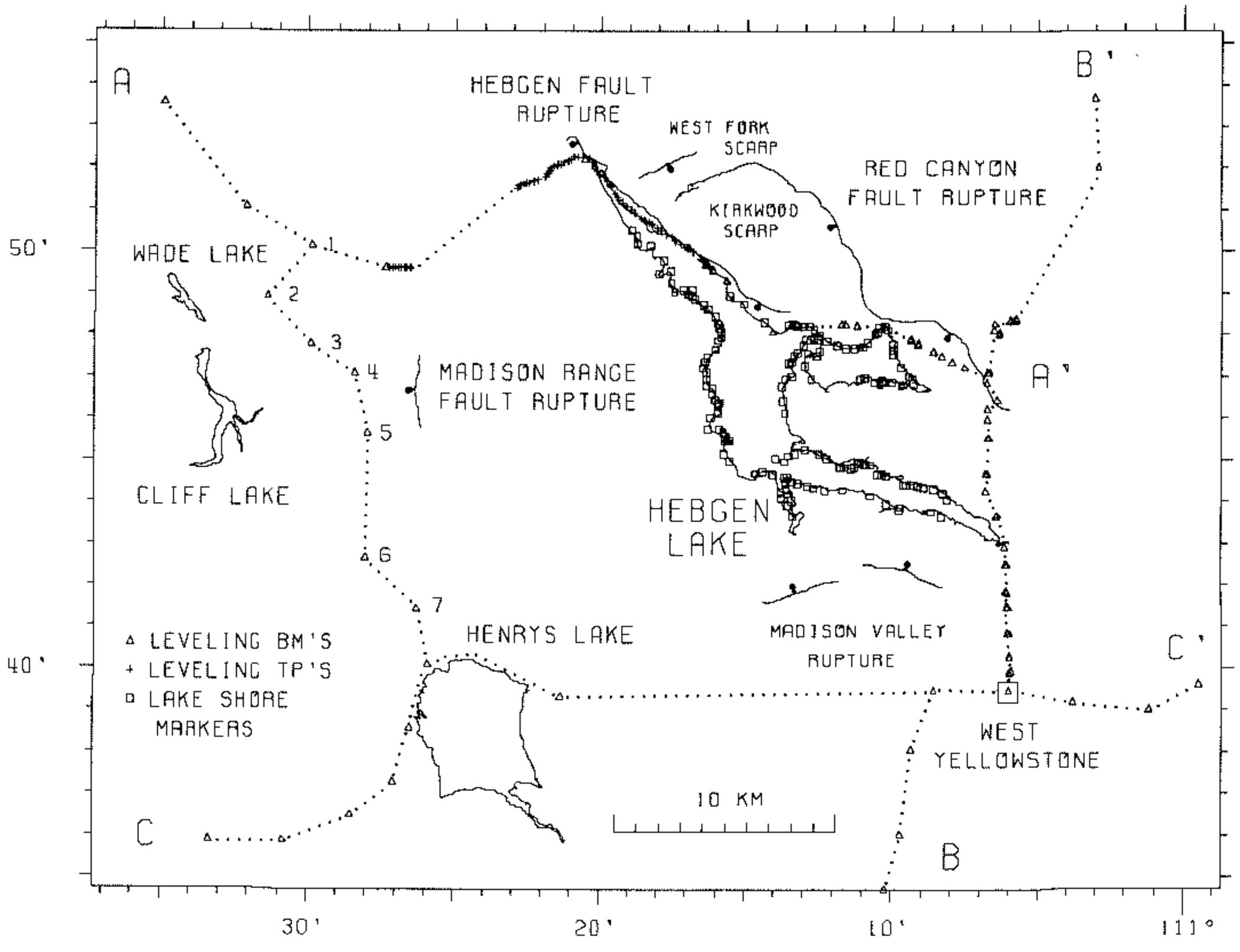

FIG. 2. Main ruptures and data distribution at Hebgen Lake. Line A-A′ is based on leveling bench marks (triangles) and leveling turning points (crosses). Two other lines, B-B′ and C-A, consist of leveling bench marks. Squares represent lake shore height changes.

The Hebgen Lake earthquake occurred beneath two short northwest-trending overlapping faults that closely follow Laramide thrust contacts. The normal faults are part of a system that has more than 600,000 yr of age but less than 2 m.y., as inferred by Christiansen (1986) from displacements of ash flow tuffs, and lie only 30 km from the Yellowstone Caldera rim. A 5 km-long segment of the north trending Madison Range fault also ruptured during the 1959 earthquake (Figure 2). Antithetical slip on late Quaternary faults south of Hebgen Lake, studied by Nash (1984) and Myers and Hamilton (1964), may be the easternmost extension of the east-trending Centennial fault (Myers and Hamilton, 1964; Christiansen, 1986). Thus, four faults with three different orientations slipped during the event, all at locations close to the site of magma injection into the upper crust.

THE 1959 HEBGEN LAKE, MONTANA, EARTHQUAKE

Data

Four types of data were collected to analyze the static deformation field associated with the 1959 Hebgen Lake earthquake: National Geodetic Survey leveling lines, highway turning points, lake shore data, and fault scarp offsets. Figure 2 shows the 1959 fault scarps along Hebgen and Red Canyon faults on the northern side of the lake and the data distribution. The three leveling lines, routes A-A′, B-B′, and C-A (lines 1, 2, and 3, respectively), are denoted by dots. Highway turning points are marked by crosses on line A-A′. Lake shore elevation changes are the squares along

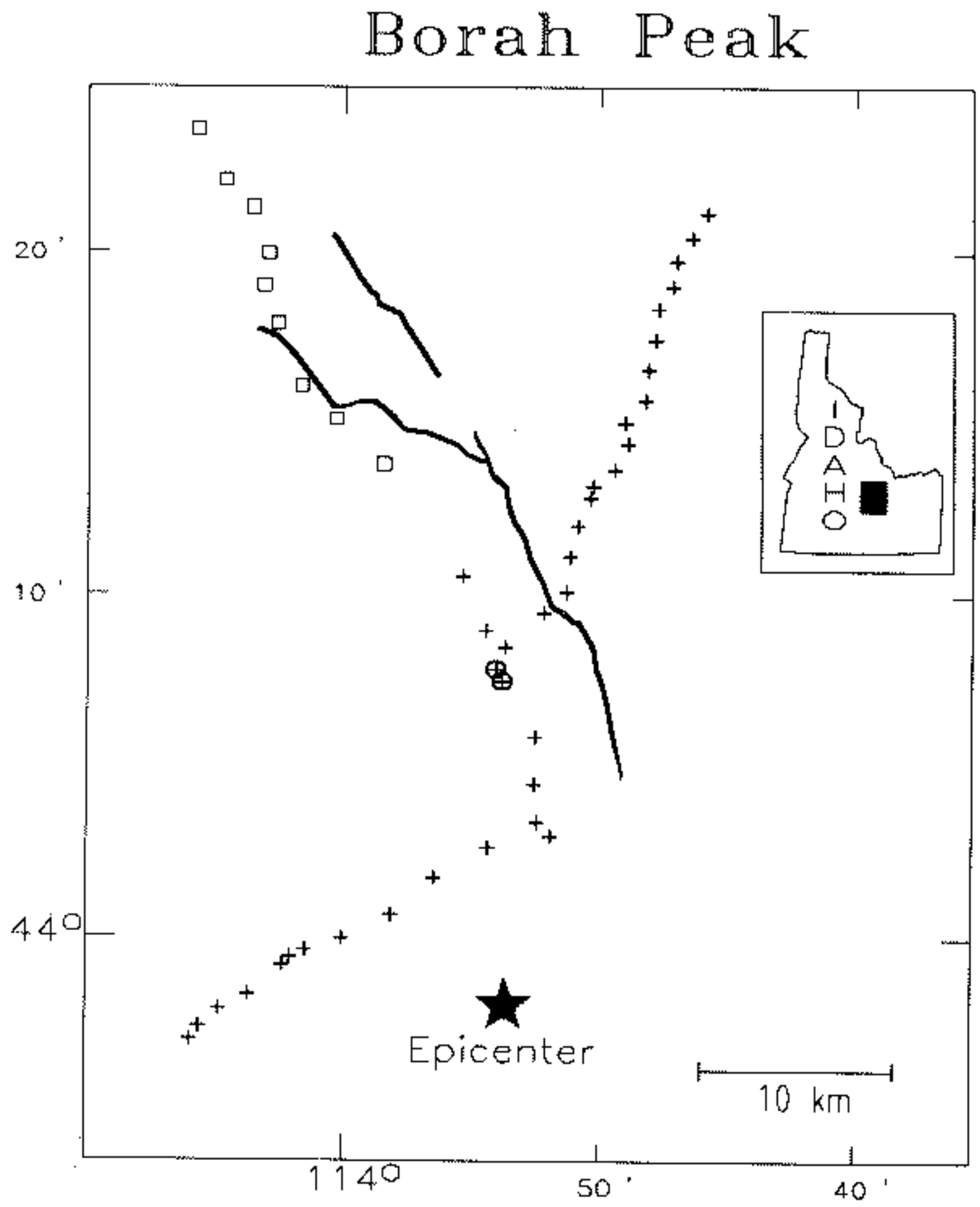

FIG. 3. Map view of the leveling route showing bench marks and the newly ruptured segment of the Lost River fault at Borah Peak. Bench marks (crosses and squares) southwest of the fault were leveled in 1933. Those to the northeast (crosses) were leveled in 1948. All of them were releveled in 1985. The circled bench marks are the two common points of the 1933 and 1948 routes. The squares are newly gathered observations. The star marks the epicenter determined from seismic data (Richins *et al.*, 1985).

TABLE 1

ERRORS IN HEBGEN LAKE DATA

Data Type	Error
Leveling*	$\alpha L^{1/4} \times 10^{-3}$ m (random error) $20 \times 10^{-6}\ \Delta h$ m (residual rod error) $40 \times 10^{-6}\ \Delta h$ m (residual refractory error) Average = 15 mm
Highway turning points	~0.3 m
Lake shore	~0.08 m for values ≦ 4.7 m ~0.6 m for values > 4.7 m
Fault scarp	0.9–1.5 m
rms signal = 2072 mm rms pure error = 176 mm	

* Δh and L are the topographic height difference, and the distance from a reference bench mark, respectively. α is given in Table 2.

the lake boundary. The estimated precision of all of these measurements are summarized in Table 1.

Leveling lines. Leveling data have been divided into preseismic (1923 to 1948 surveys) and postseismic (1959 to 1964 surveys) groups. Differences in elevations, topography, and estimated errors (discussed below) along the three lines are shown in Figures 4, 5, and 6 for lines 1, 2, and 3, respectively. The zero level of elevation change along these four lines has been taken as the asymptote of the signal for distances greater than 50 km from the lake.

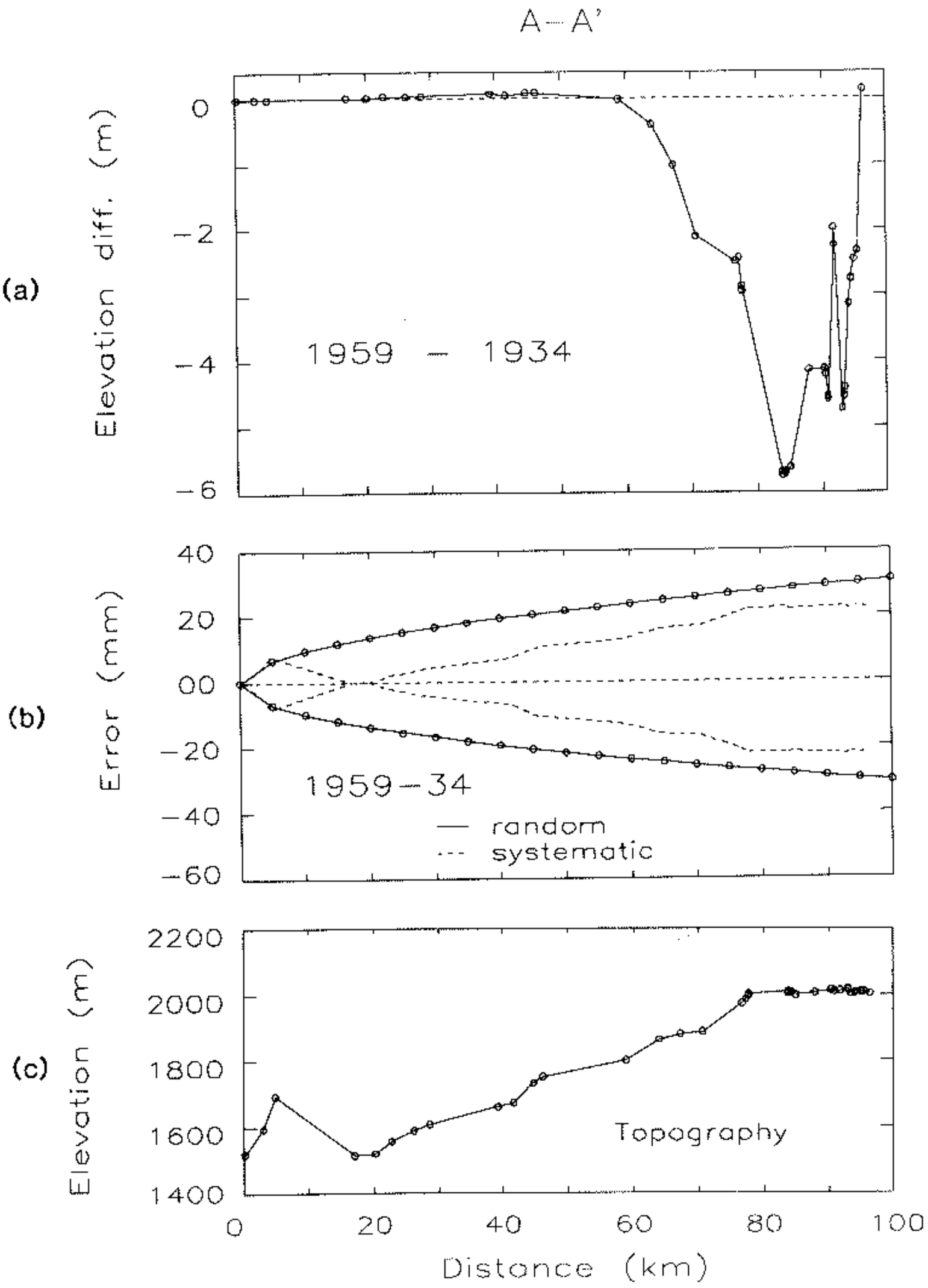

FIG. 4. (a) Elevation change at Hebgen Lake between the 1959 and 1934 surveys along the A-A′ profile of Figure 2. (b) Errors associated with the elevation change in A-A′. Solid line is the envelope of the random errors which propagate as the square root of distance. Dashed line is the combination of residual rod and refraction errors. (c) Topographic relief along the route.

All first and second order data have been corrected for level collimation, rod excess, and rod thermal expansion. The atmospheric refraction correction was estimated using the REDUC4 program of Holdhal (1981). Table 2 shows line number, National Geodetic Survey designation, survey specification, and standards of each survey. The standard deviation β obtained in repeated measurements of the same sections of a line gives a good indication of the random errors for adjacent bench marks. Bomford (1971) states that the random error σ should propagate as $\sigma = \alpha L^{1/2}$, where σ is in millimeters, α is a function of β, and L is distance in kilometers. If the survey is double run with a bench mark spacing of 1 km, then β should be about one-third of the rejection tolerance. This relation can be seen in Table 2. If β follows a Gaussian distribution, then $\alpha \approx \beta$. The propagation of random errors in the elevation changes (postearthquake less preearthquake elevations) is determined by $\alpha_T = \sqrt{\alpha_1^2 + \alpha_2^2}$, where α_1 and α_2 are the corresponding values for the pre- and postearthquake surveys. When dealing with lines composed of more

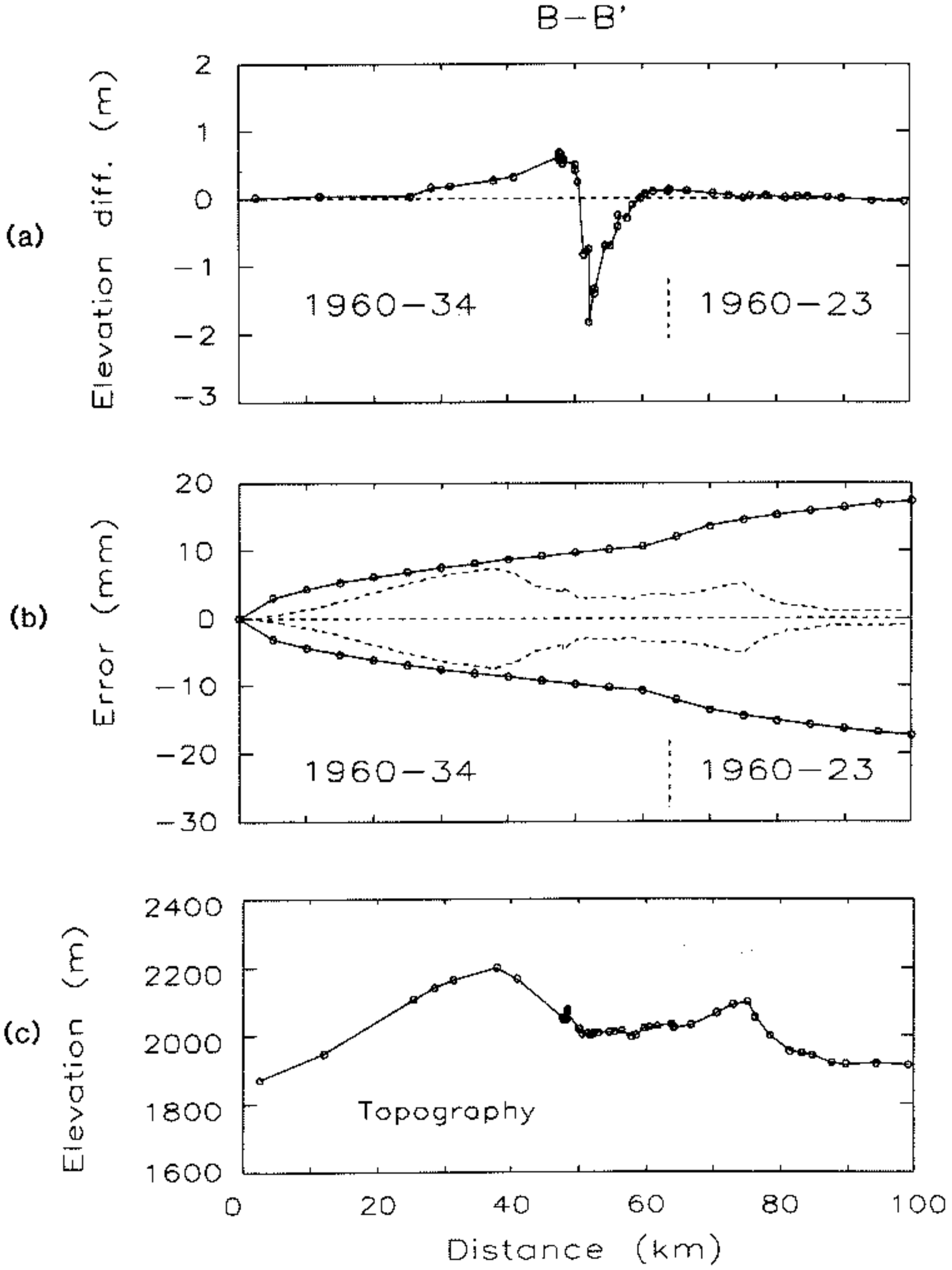

FIG. 5. Same as Figure 4, for line B-B'.

than two surveys, α_T changes at the location where the surveys meet. Figures 4b, 5b, and 6b show the envelopes of the random errors (solid lines) associated with leveling lines 1, 2, and 3. The residual rod and refraction errors, after correction using the rod calibration certificates and temperatures measured at each section, are estimated to be $20 \times 10^{-6}\ \Delta h$ m from Stein (1981), and $40 \times 10^{-6}\ \Delta h$ m from Stein *et al.* (1986), where Δh is topographic height difference along the profile (bottom panels of Figures 4 to 6). These two residual errors are combined following the law of error propagation $e_T = \sqrt{e_1{}^2 + e_2{}^2}$ and are plotted as dashed lines in Figures 4b, 5b, and 6b.

The coseismic elevation differences span a 30-yr period, and thus includes possible deformations preceding and following the 1959 event. Reilinger (1977, 1985, 1986) has argued that significant deformation followed the earthquake. Savage *et al.* (1985) measured large horizontal extension normal to the fault (0.3 ppm/yr) during 1973 to 1984. We conducted two tests of intrasurvey movement during the periods 1934 to 1948 (preseismic) and 1959 to 1964 (postseismic) for the loop around the lake. The tests revealed negligible aseismic deformation and yielded random errors consistent with the *a priori* error estimates.

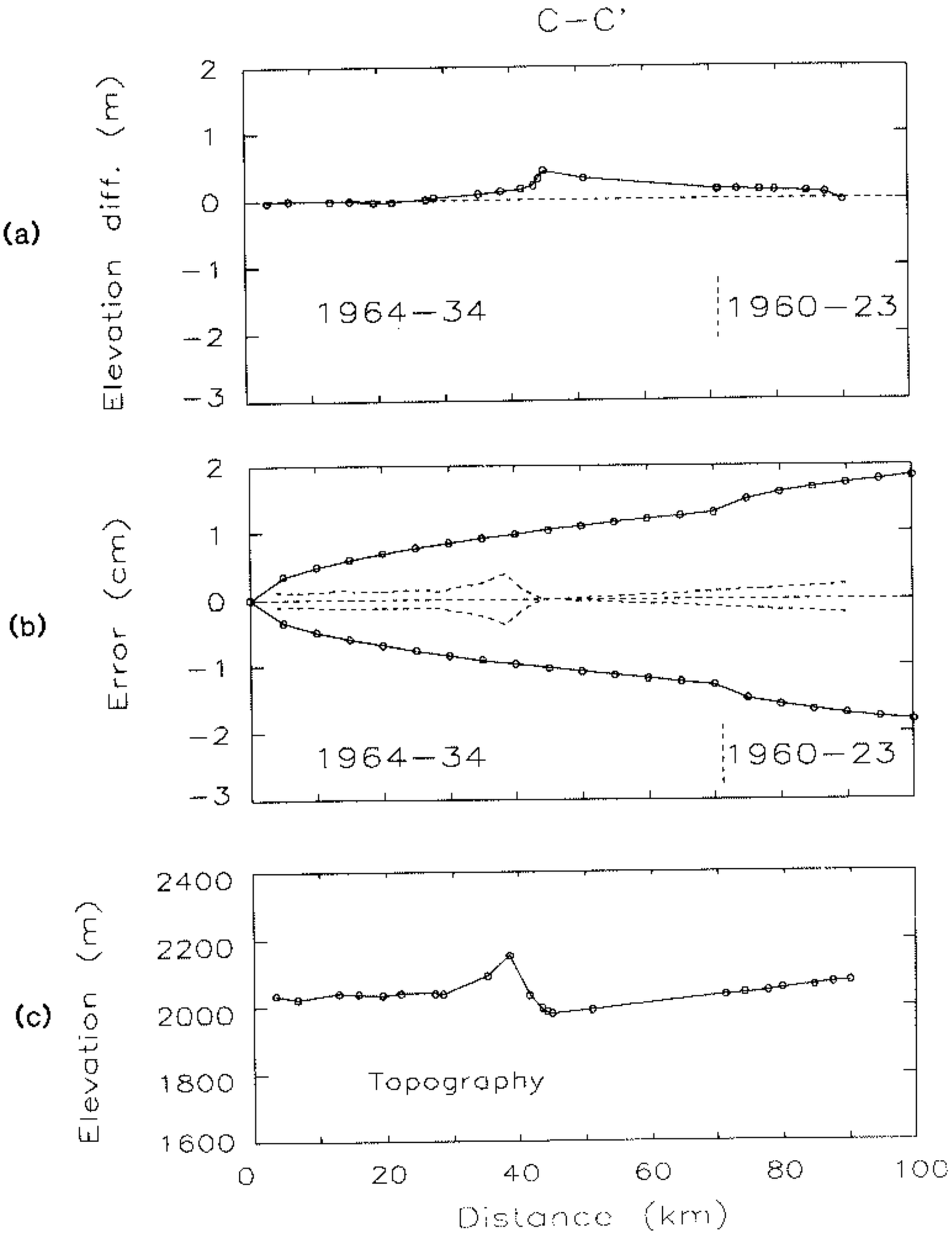

FIG. 6. Same as Figure 4, for line C-C′.

Movement during a 14-yr period before the earthquake (1934 to 1948) and a 5-yr period after the shock (1959 to 1964) can be assessed by the misclosure of the circuit that skirts the epicentral region. This procedure has been applied by Chi *et al.* (1980) to investigate vertical crustal movements in Western United States. We recovered third order double-run leveling along the C-A profile that closed the loop around Hebgen Lake (bench marks labeled 4, 5, 6, and 7 in Figure 2). Bench marks 2 and 3 were releveled in September 1986, tied to bench marks 1 and 4, and were not included in the following misclosure analysis. The preseismic circuit consists of the 1934 NGS lines L2986, L2992, L2997 and the USGS 1948 MV152a line. The −68.6 mm (clockwise) misclosure over the 106.2 km circuit indicates a value of α_T = 6.6 mm/km$^{1/2}$. A composite value of $\hat{\alpha}_T$ can be predicted from each individual α (from Table 2) as $\sqrt{\alpha_1^2 + \cdots + \alpha_n^2}$. For the loop, $n = 4$ and $\hat{\alpha}_T = 5.6$ mm/km$^{1/2}$. The postseismic loop was closed using the 1959 NGS line L17565, the 1964 line L19913, and the U.S. Geological Survey 1963/64 PV508a/568a. The −47.1 mm postseismic closure indicates a value of $\alpha_T = 4.6$ mm/km$^{1/2}$. In this case, $n = 3$ and $\hat{\alpha}_T = 7.8$ mm/km$^{1/2}$. Values of $\hat{\alpha}_T$ thus predict the random error present in the total composite line. Because the observed misclosure is about the same as that estimated by propagation of random errors, intrasurvey movement during 1934 to 1948 and

TABLE 2

HEBGEN LAKE LEVELING SPECIFICATIONS

Line No.	NGS Line HGZ	Survey Period	Double or Single Run	Order of Leveling	Rejection Tolerance (mm)	S.D. β (mm)	α_T (mm)
Line 1	L2986	Oct. 1934	Single	Second	8.4	2.80	3.06
	L17565	Sept. 1959	Double	First	4.0	1.24	
Line 2	L2992	Oct. 1934	Single	Second	8.4	2.38	2.74
	L18104	Aug.–Sept. 1960	Double	First	4.0	1.36	
	82410	Oct.–Dec. 1923	Double	First	4.0	1.60	2.11
	L18004	July–Aug. 1960	Double	First	4.0	1.37	
	82414	Oct. 1923	Double	Second	8.4	1.47	1.95
	L18098	Sept. 1960	Double	First	4.0	1.28	
Line 3	L2997	Sept. 1934	Single	Second	8.4	2.80	3.08
	L19913	Sept.–Oct. 1964	Double	First	4.0	1.29	
	MV152a*	July–Aug. 1948	Double	Third	12.0	3.25	8.26
	PV508a/568a*	July 1963–Oct. 1964	Double	Third	12.0	7.6	

* Third-order surveys performed by the U.S. Geological Survey.

1959 to 1964 was small (<50 mm) or nonexistent in the vicinity of the earthquake. A broad uplift of the entire area as suggested by Reilinger (1977) cannot be detected with this test.

Postseismic error can also be assessed by examining bench marks that were surveyed twice after the earthquake. A 15-km segment of the line B-B′ (from BM 5 EI109 USDA to 5 EI138 USDA in Figure 7, a and b) was first leveled in 1934 and releveled in September 1959, in 1960, and partially in 1964. Apart from local subsidence across the fault trace, less than 10 mm of deformation occurred. In the year immediately after the earthquake, postseismic subsidence reached a maximum of 35 mm relative to neighboring bench marks. This is about 2 per cent of the maximum coseismic subsidence.

Turning point heights on the highway. When bench mark recovery was poor, the prequake elevation profile of Highway 287 northwest and west of Hebgen Lake was reconstructed by Myers and Hamilton (1964) from the heights of the base of the rods (turning points) along the road surface. The rod turning point heights and distances were recorded in the field books of the Bureau of Public Roads leveling crews, but the exact location of these points could not be recovered. Coseismic deformation was found by comparing these measurements with those obtained in the postquake survey performed by the Coast and Geodetic Survey. Myers and Hamilton (1964) estimate the uncertainty of the turning point measurements to be about 0.3 m.

Lake shore height changes. Shoreline measurements were made several weeks after the earthquake by Myers and Hamilton (1964, p. 75). The high water mark was recognized by stained rocks and posts, the limit of the beach sand, cuts in unconsolidated material, and grounded driftwood. The submerged former shoreline was determined on the basis of submerged trees, shrubs, and plants. Since the lake level was recorded daily at the tide gage on Hebgen Dam, these measurements were tied to the leveling lines. Where the postquake lake level was lower than the prequake level, the difference could be easily established, and the uncertainty was estimated to be of the order of 0.06 m (Myers and Hamilton, 1964). In those cases where the prequake lake level was submerged after the earthquake, two different uncertainties were associated to these measurements: 0.08 m for values of subsidence less than 4.7 m and 0.6 m for subsidence greater than 4.7 m.

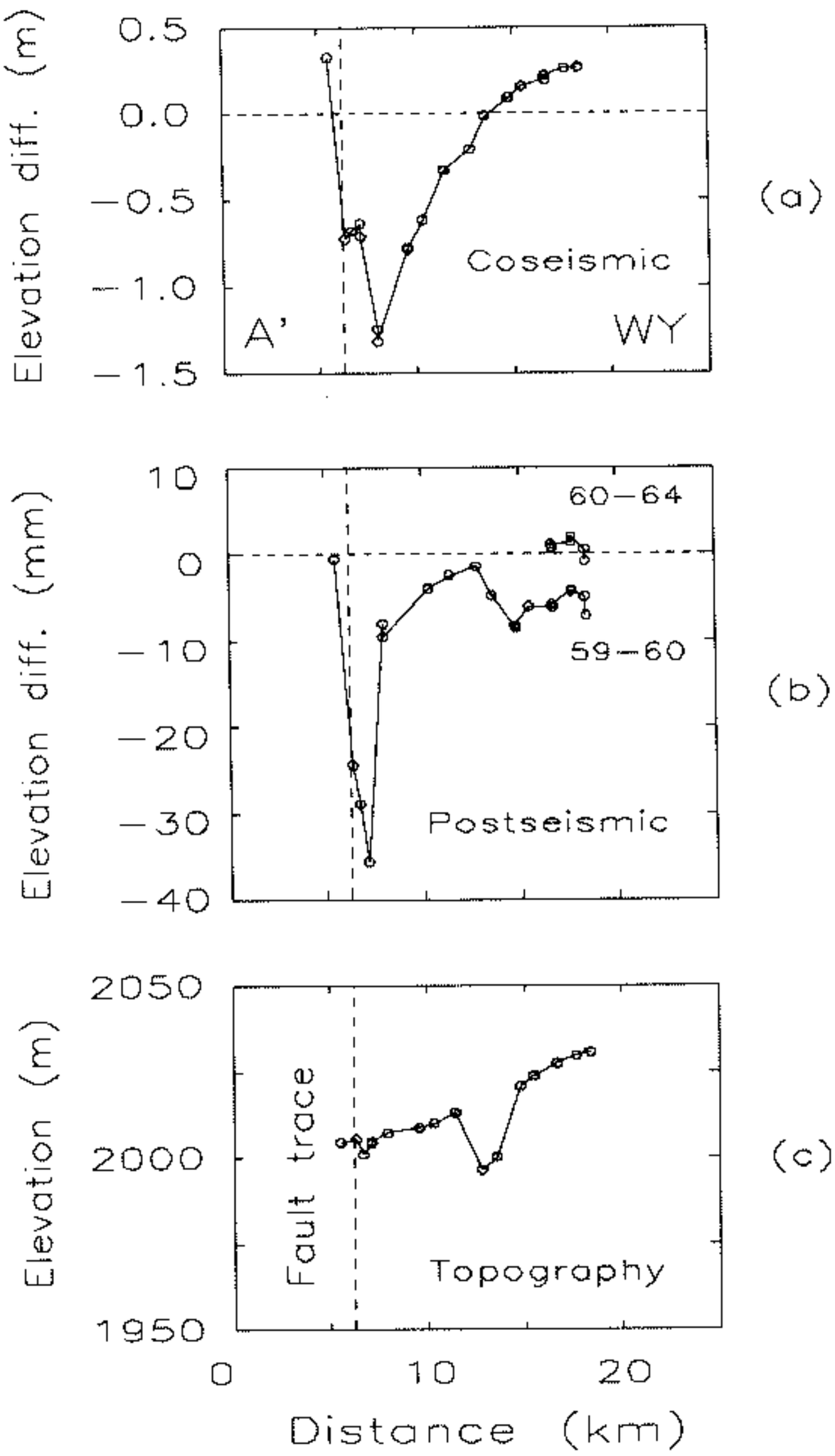

FIG. 7. Comparison of the coseismic (1934 to 1959) deformation at Hebgen Lake (a) with two intervals of postseismic (1959 to 1960 and 1960 to 1964) deformation (b) along a segment of the B-B′ line. Vertical dashed line is the intersection of the survey line with the Red Canyon fault trace. Localized subsidence of 35 mm is restricted to 1 to 2 km from the fault. Topography along this segment (c).

Fault scarp measurements. Ruptures on the Hebgen, Red Canyon, and Madison Range fault scarps were associated with the Hebgen Lake event (Figure 2). The Hebgen scarp is roughly linear, 12 km long, and runs parallel to the northeastern shore of the lake. The fault had a maximum vertical displacement of 6.7 m. It dips southwest between 60° ~ 85° at the ground surface with the southwest block downthrown. The arcuate Red Canyon scarp extends for about 22 km with a maximum vertical displacement reaching 4.7 m near its mid-point. Its southwest dip varies from 50° to 85°. Both of these scarps share the trace of older faults.

Secondary features in the area are the West Fork and Kirkwood scarps. They are roughly linear, 3 km long, and locate at the northwestern end of the Red Canyon scarp. Maximum vertical displacement on these secondary scarps reached 1.2 and 0.6 m, respectively. Minor scarps and fissures with maximum vertical displacements up to 0.2 m were produced in the Bull Lake glacial moraine (4 to 5 km south of Hebgen Lake, Figure 2). A new scarp was formed on the prehistoric fault that runs along the western side of the Madison Range near Missouri Flats (Figure 2). This new feature extends for over 4 km with a vertical displacement up to 1 m.

Witkind, Epstein, Myers, Hamilton, and Hayes (U.S. Geological Survey, plate 2, 1964) gave values of scarp displacements corrected for the ground slope, grabens, subsidiary fractures, and local slumping. The uncertainties of the vertical displacement (throw) are 0.9 to 1.5 m (Witkind, oral communication, 1986).

Turning points on Highway 287, lake shore height changes, and fault scarp offsets were digitized from plate 2 of Myers and Hamilton (1964).

Planar Fault Models with Uniform Slip

Single plane

The dislocation surface is simulated by the superposition of point sources uniformly distributed over the fault plane. The fault surface is characterized by its dip angle, length along strike, and length in the down-dip direction (width). The strike and the location of one end of the fault are also required to specify the position of the fault plane. Expressions for the vertical displacement resulting from a static moment tensor buried at a given depth can be found in Okada (1985) or Ward and Barrientos (1986). The average displacement, $\bar{u}$, is estimated by dividing M (scalar moment) by $\mu \Delta S$, where μ is the rigidity and ΔS is the fault area.

We searched by trial and error for the parameters that best satisfy the data in the least-squares sense, inverting for the magnitude of pure dip-slip. Because the data present unequal uncertainty, the inversion is weighted, with weights inversely proportional to the variances of measurement error (see Table 1).

The best single plane is shown in Figure 8. The average displacement is 11 m. Because the northwestern extension of the fault is poorly constrained by the westernmost points of line 1, the length along strike ranges from 18 to 30 km, accepting a 10 per cent variance increase. Data of line 2 (B-B′) constrain the southeast corner position and the depth of burial of the fault plane at the intersection of this line with the fault plane, and the lake data constrain the fault dip to 50° ± 5° and width to 13 to 20 km, corresponding to a vertical depth extent of 10 to 16 km. The total moment is 1.3×10^{20} N-m (for $\mu = 3.23 \times 10^{10}$ Pa). These values are not significantly different from those obtained by Savage and Hastie (1966), although they considered a fault striking about N110°E [according to the focal mechanism obtained from P-wave polarities by Ryall [1962)]. This study suggests a plane strike of N126°E.

The weighted rms misfit is given by $\left[\frac{1}{N-K} \sum_{i=1}^{N} r_i^2 w_i^2\right]^{1/2}$, where the residual $r_i = o_i - c_i$ is the difference between observed and predicted elevation changes. $N = 170$ is the number of data points, and K is the number of independent parameters. w_i is defined as $\bar{\sigma}/\sigma_i$ where σ_i^2 is the uncertainty of the ith observation point, and $\bar{\sigma}^2 = N \left[\sum_{i=1}^{N} \sigma_i^{-2}\right]^{-1}$. The rms pure error is defined as $\left[\frac{1}{N} \sum_{i=1}^{N} \sigma_i^2\right]^{1/2}$. The rms signal to be modeled is 2072 mm, and the rms pure error is 176 mm. Thus, the rms signal-to-noise ratio is 12. The single-plane model produced 726 mm rms misfit, four times greater than the pure error.

Two planes

Following the strategy used for the single-plane model, we inverted for slip on two different faults. The location and strike of both fault planes were perturbed around the mapped Hebgen and Red Canyon faults to satisfy the large elevation changes along line 1. The best two-plane uniform slip model is shown in Figure 9.

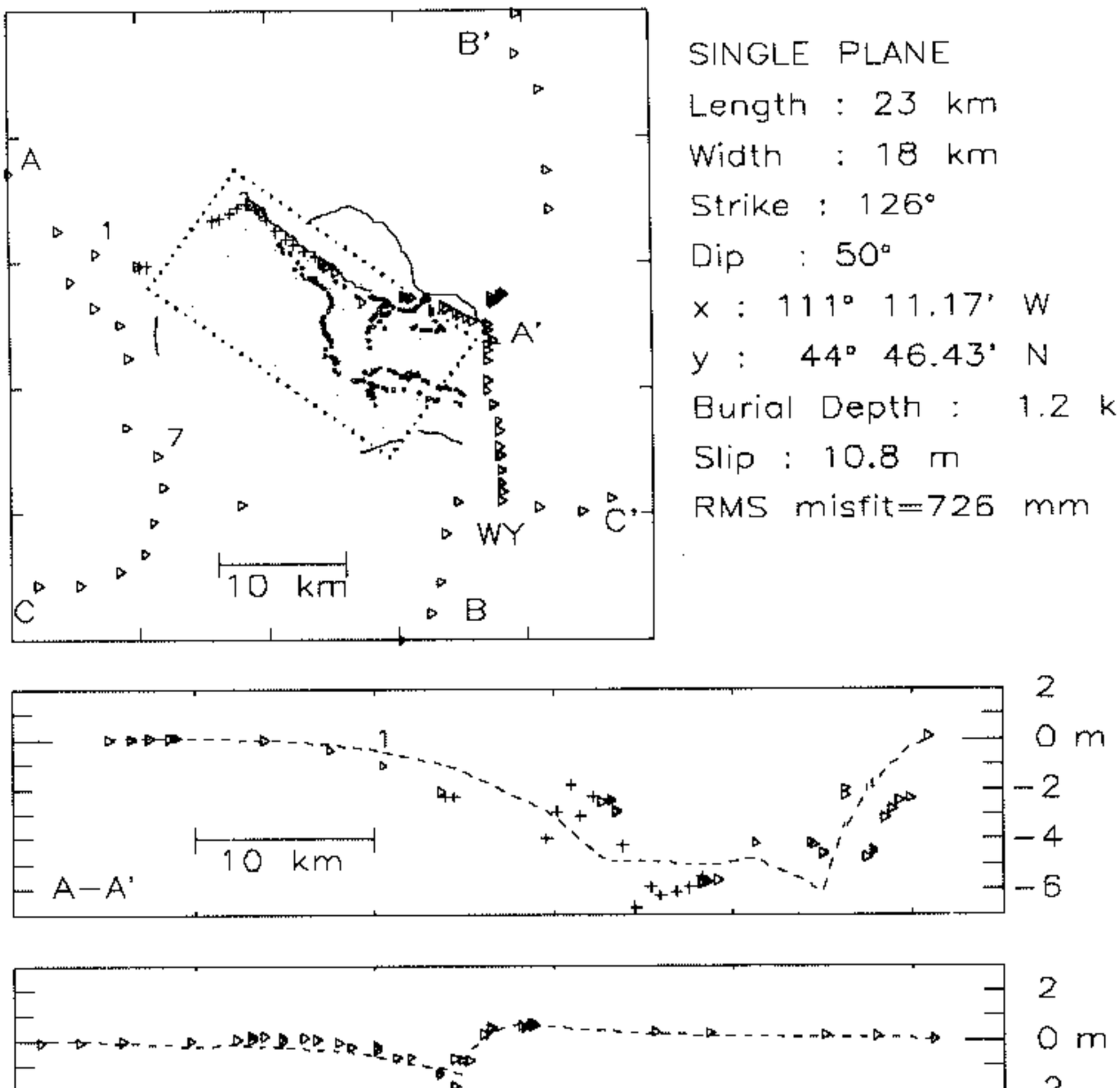

FIG. 8. Best single-plane model for Hebgen Lake. The *upper box* shows the data distribution and the surface projection of the fault plane. Observations and predicted vertical elevation change (dashed) along the lines A-A′, B-B′, and C-A. Two projections of lake shore height changes (circles) are compared with the theoretical values in the *lower box*. Misfits of bench marks (triangles) and turning points (crosses) along the lake and line A-A′ suggest a multi-planar source.

Given the added degrees of freedom to the two-plane inversion, is the improvement in fit over the single plane significant? To compare the variance of misfits of two models, we construct the ratio

$$F = \frac{(SSR_1 - SSR_2)/(\nu_1 - \nu_2)}{SSR_1/\nu_1}$$

to analyze the $F_\alpha(\nu_1, \nu_2)$ statistic (e.g., Langbein *et al.*, 1983). The quantities SSR_1 and SSR_2 represent the weighted sum square of residuals for the single-plane and two-plane model. ν_i is the number of degrees of freedom of the ith model, ν_1 is $(f_1 - f_2)$, and $\nu_2 = N - f_1 - 1$, where N is the number of observations and f_i is the number of free parameters of the ith model. The sum square of errors dropped from

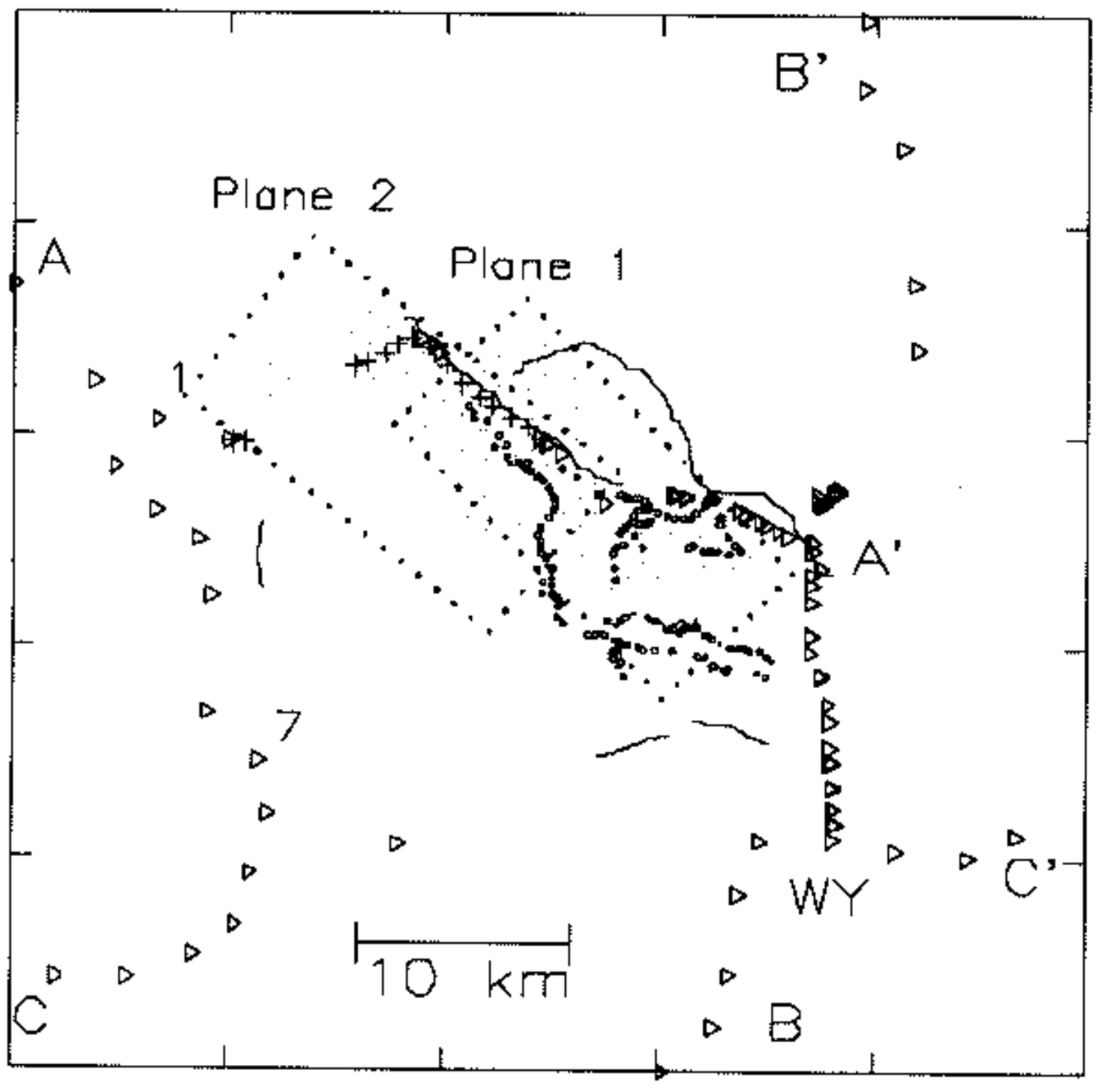

FIG. 9. Same as Figure 8 for the two-plane model. Two overlapping fault planes that closely follow the rupture traces and dip 45° and 50° best satisfy the observations.

165 to 37 m^2 when 9 degrees of freedom were added. $F = 13.3$ is significant at the 99 per cent confidence level. Thus, the two-plane model fits the data significantly better than the single-plane model.

Characteristics of the southeastern (fault 1) and the northwestern (fault 2) planes

include: slip on fault 1 is similar to that on fault 2 (7.8 to 7.0 m). The associated scalar moments are 5.2×10^{19} and 6.8×10^{19} N-m. The 1.2×10^{20} N-m combined moment is very close to that given by the single-plane uniform slip model. The southeast corner and depth of burial of fault 1 at the intersection with line 2 is well-constrained. Changes in strike of fault 1 (128° to 143°) can be compensated by perturbing the plane location by a few kilometers without altering the overall fit. Plane 2 dips 50° ± 3° to the southwest. Plane 1 dips 45° basinward. Greater values (50°) increase the sum square of residuals (to 41 m^2) but tend to reduce the systematic misfit along line 2 (B-B′). The extent of both planes is well-constrained to the southeast but poorly constrained to the northwest, particularly plane 2. Values of fault length vary from 15 to 25 km. Downdip widths are 9 to 16 km for plane 1 and 11 to 18 km for plane 2.

The observed scarp heights along the Red Canyon and Hebgen faults (solid line) can be compared to the predicted slip from the uniform slip model (dashed line) in Figure 10 (top). The model overestimates the surface slip along both faults, particularly at the western end of the Hebgen fault, where the model predicts about 7 m and no surface breakage was detected. In this region, the Paleozoic limestone that the normal and Laramide thrust faults both follow no longer crops out at the surface.

Seismicity in the Hebgen Lake region during 1973 to 1981 is presented in Figure

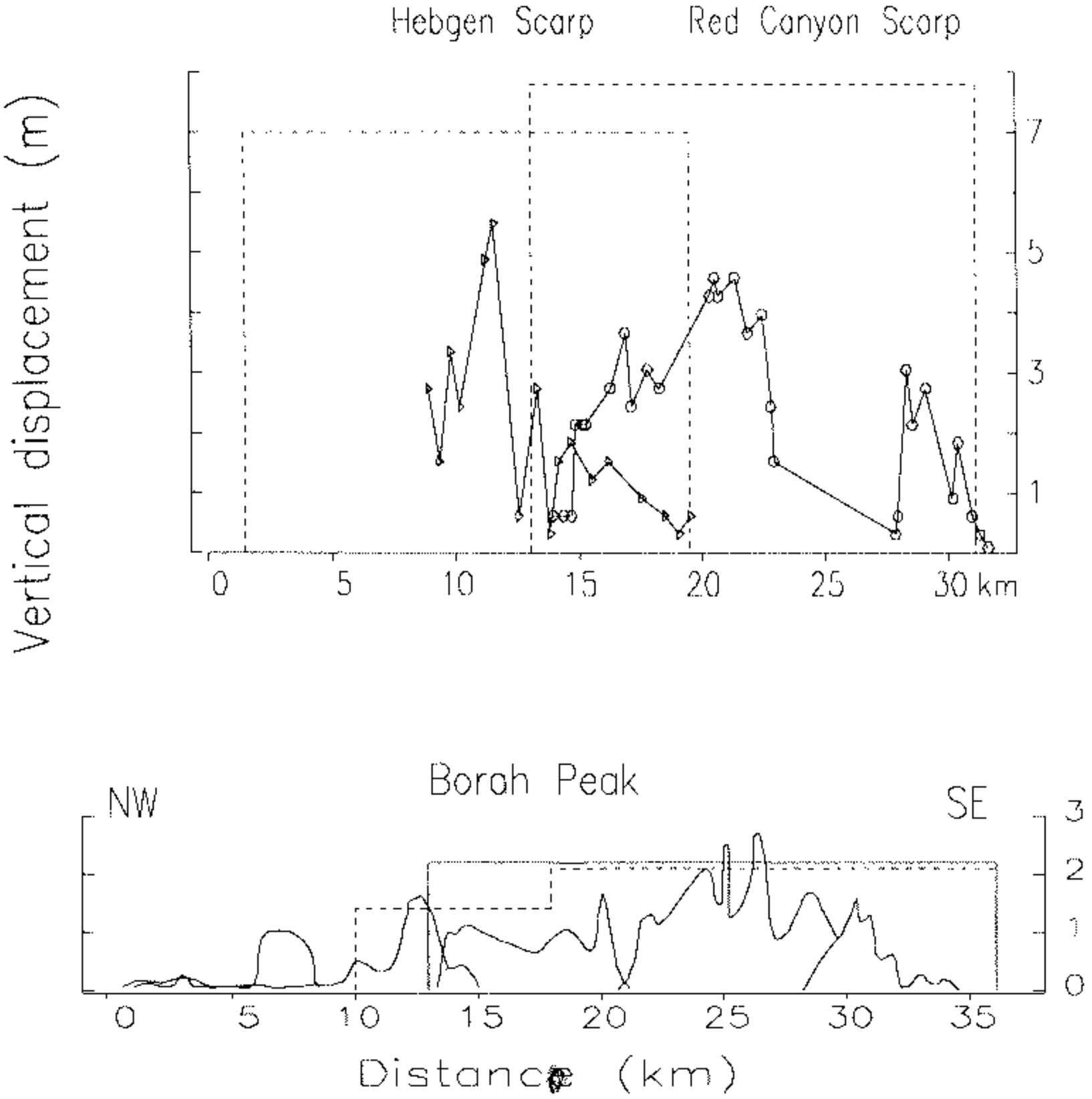

FIG. 10. (*Top*) Fault scarp offsets at Red Canyon (circles) and Hebgen faults (triangles) compared to the predicted vertical displacement of the two-plane model (dashed). (*Bottom*) Observed (solid line) and predicted fault scarp offsets at the 1983 Borah Peak ruptured segment. Constant slip of 2.2 m is predicted by the single-plane model (constant solid line). The two-plane model predicts 2.1 m toward the SE and 1.4 m at its NW end (dashed line).

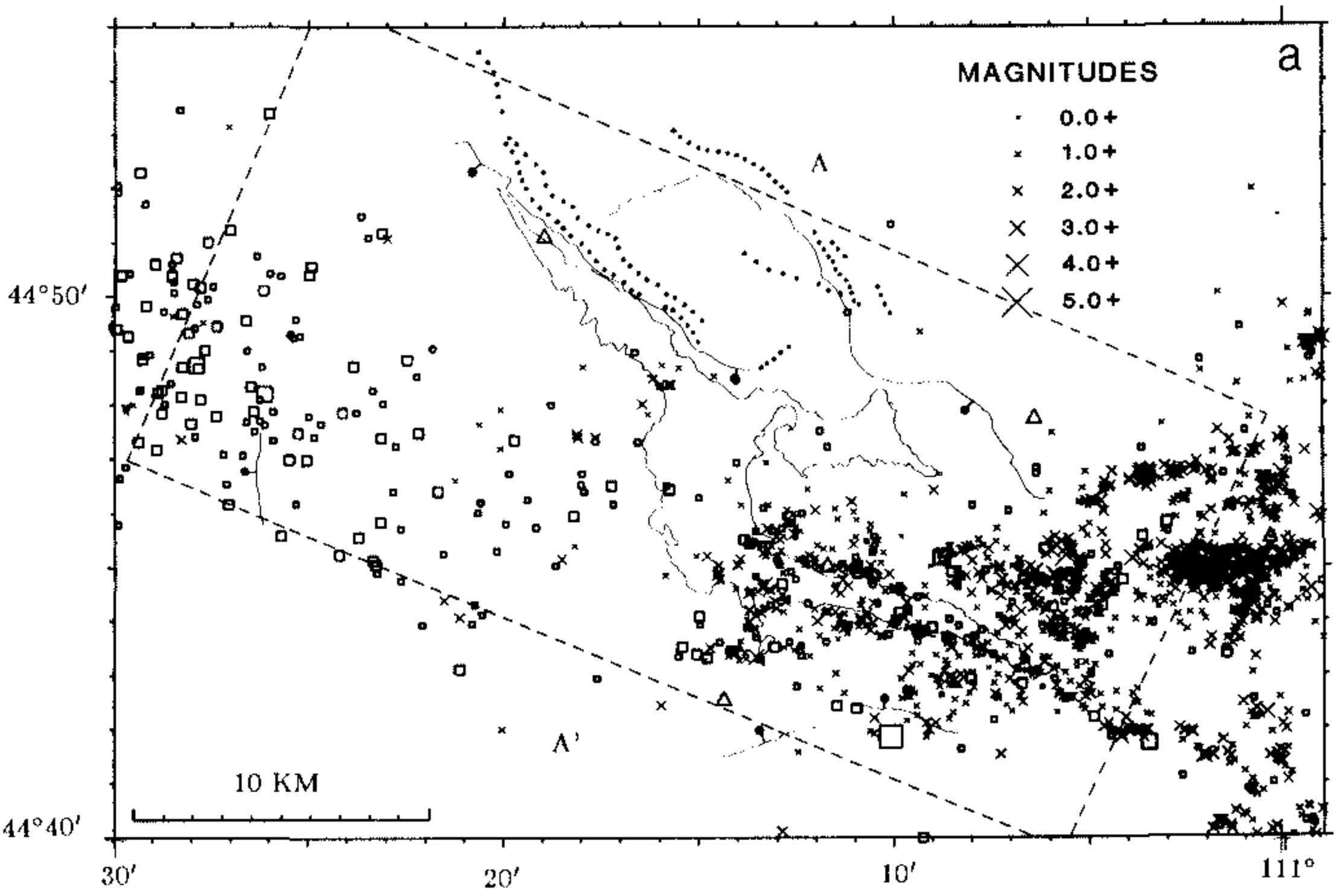

FIG. 11. (a) Seismicity of the Hebgen Lake region from 1973 to 1981 (Pitt, 1987) and seismograph stations (triangles) superimposed over the lake and the 1959 ruptures (solid lines are normal faults and dots represent thrust faults). (b) Cross-section along A-A′ showing the best two-plane coseismic model. Only epicenters within the dashed box and location quality A and B are plotted. (c) Same as (b) with the listric model. The curved plane abuts the planar fault at a depth of 8 km.

11a, after Pitt (1987). The epicentral distribution of these events (locations with qualities A, B, and C) is similar to aftershocks recorded for the period 1964 to 1972 in Eaton *et al.* (1975). Unfortunately, station coverage before 1973 was too sparse to compare hypocentral locations. Figure 11b superimposes the best two-fault planar

model on a cross section of the 1973 to 1981 hypocenters (quality A and B locations only) normal to both faults. Events concentrate on the southeastern half of plane 1, leaving plane 2 depleted of aftershocks.

Doser (1985) analyzed the source process, fault geometry, and hypocenters of the main shock and the larger aftershocks of the Hebgen Lake event. She concluded that the main sequence was the result of two subevents of magnitude $m_b = 6.3$ ($M_0 = 3 \times 10^{18}$ N-m) and $m_b = 7.0$ ($M_0 = 1 \times 10^{20}$ N-m) separated by 5 sec. The larger shock occurred at 15 ± 3 km depth with a dip of 50° ± 5° from long-period data and 60° ± 5° from short-period polarities. Doser (1985) finds 10 to 20 km uncertainties associated with the epicenter location of the main shock, but estimates that the second event of the sequence occurred 5 to 8 km south of the first.

Madison Range fault. Newly recovered leveling data (bench marks 2 to 7, north of Henrys Lake, Figure 2) allow us to bracket the coseismic slip on the Madison Range fault (Figure 1) which showed about 1 m of surface offset during the 1959 earthquake and about 11 m of post-Pinedale (<15,000 yr) movement (Mathieson, 1983) along a 15-km segment centered on the 1959 rupture. Doser (1985) reports that a 23 November 1947 shock occurred on the Madison fault about 10 to 15 km north of the 1959 rupture, with a Modified Mercalli intensity VIII ($M_L > 5.5$). Part of this fault was reactivated during the 1959 event forming a new scarp nearly 4 km long (Figure 2). The reactivated segment shows concentrated seismicity during 1973 to 1981 that may, however, be aftershocks. The formation of this new scarp and the east-west topographic relief of the Hebgen Lake Basin, Madison Range, and Missouri Flats (between Madison Range and Cliff Lake, Figure 2) led Fraser *et al.* (1964) to postulate the "dual-basin" concept. They proposed that during the 1959 event, the Hebgen Lake basin subsided 2 to 6 m and that the basin on the downthrown block of the Madison fault subsided 1 to 2 m. Instead, the subsidence measured at bench marks 4 and 5 (Figure 2) is less than 0.5 m and is localized to the 1959 scarp.

To quantify permissible slip on the Madison Range fault, we included a third plane in the inversion procedure. The length (12 km) and strike (180°) of this plane coincides with the late Quaternary fault scarp that runs along the west front of the Madison Range (Christiansen, 1986). We fixed the dip at 50° to the west, the width to 12 km, and inverted simultaneously for the dip-slip on the Madison, Hebgen and Red Canyon faults. The slip on the Madison Range segment required by this model is 0.6 ± 0.5 m and reduces the variance for all data by ~5 per cent, which is not statistically significant. The observed coseismic deformation permits up to 1 m of deep slip ($M_0 \leqq 4.6 \times 10^{18}$ N-m) on the Madison Range fault in 1959, but does not require it.

Listric faults. Faults with dips that flatten with depth were also tested and compared to planar sources. The point source representation of the fault surface allows numerical integration of the contributions of the individual elements over a surface of any shape. For parabolic fault surfaces, a functional dependence of x and z is $x = b_1 z + b_2 z^2$, where z is depth and x is horizontal distance of each point source to the fault trace. The constants b_1 and b_2 are the fault shape parameters to be determined. They can be interpreted as the cotangent of the surface dip and the curvature of the fault. All planar faults are contained in the special case $b_2 = 0$. Listric faults with surface dip of 50° would, for example, require $b_1 = 0.85$ and $b_2 > 0$.

We systematically varied values of b_1 and b_2 for both faults of the best two-plane model covering surface dips from 35° to 80° in listric ($b_2 > 0$) and antilistric ($b_2 <$

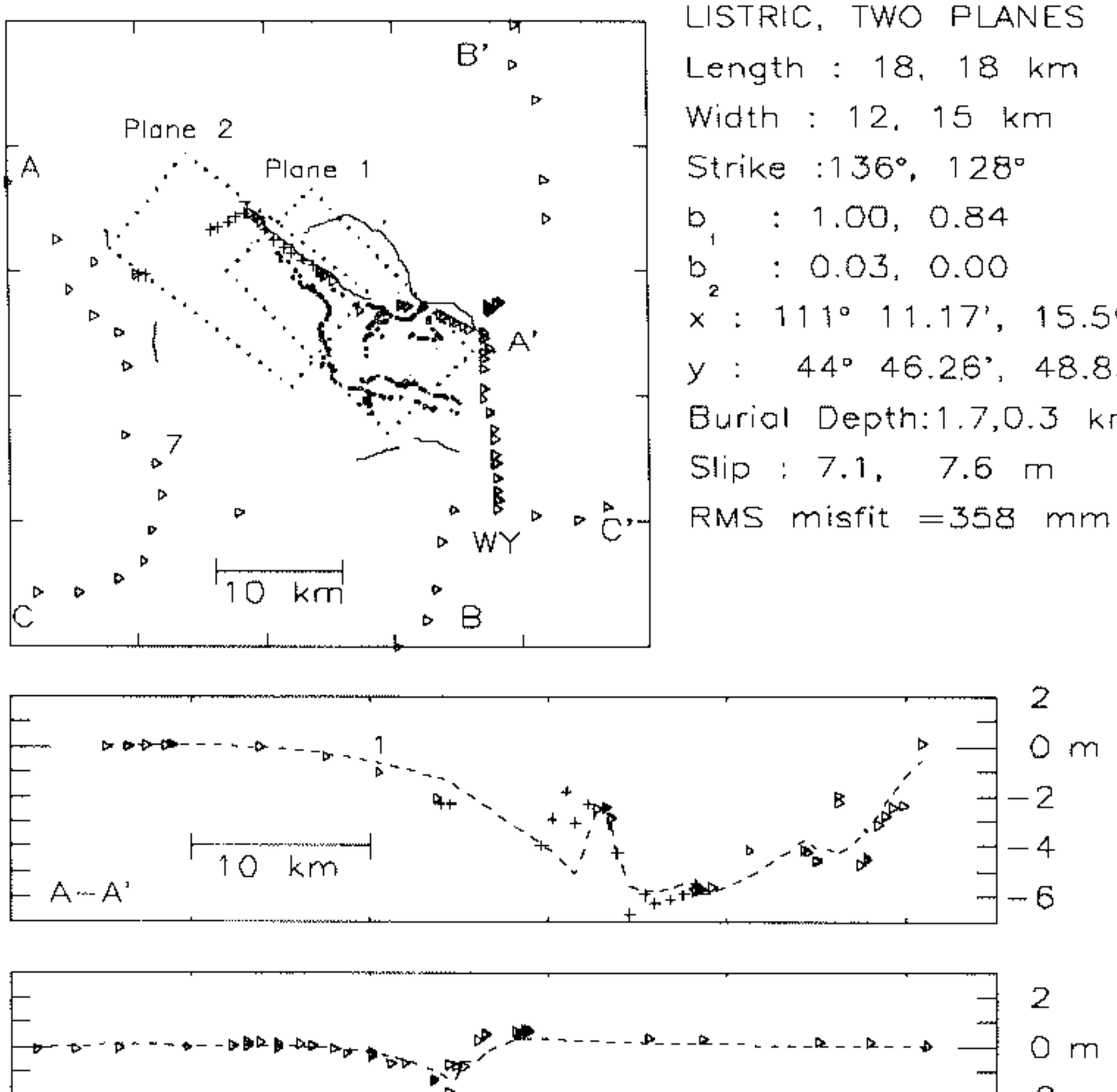

FIG. 12. Same as Figure 8 for the best listric model for Hebgen Lake.

0) cases. When plane 1 was made modestly listric, the variance of fit was reduced from 37.4 m^2 (best two-plane model) to 36.9 m^2. An F-test indicates that the increment on one degree of freedom makes the improvement not significant at the 90 per cent confidence level. No improvement of fit was observed when curvature was imposed on plane 2. The effects of the curvature with depth for fault 1 are shown in Figure 12. The curved plane 1 (Figure 11c) abuts the planar fault at a depth of 8 km, producing a wedge-shaped block. Doser (1985) proposed a similar fault geometry, based on the surface rupture and earthquake focal mechanisms of the main shock and largest aftershocks of the 1959 event.

1983 BORAH PEAK, IDAHO EARTHQUAKE

Data

Two types of data are used to analyze the deformation associated with the Borah Peak event: leveling lines and fault scarp offsets. The preseismic (a combination of

TABLE 3

BORAH PEAK LEVELING SPECIFICATIONS

Line No.	NGS Line HGZ	Survey Period	Double or Single Run	Order of Leveling	Rejection Tolerance (mm)	S.D. β (mm)	α_T (mm)
Line 1	L951	Oct.–Nov. 1933	Double	First	4.0	1.83	
	L12785	Aug. 1948	Single	Second	8.4	2.8	3.3
	L24906	June 1985	Single	First	4.0	0.49	
Line 2	L951	Oct.–Nov. 1933	Double	First	4.0	1.83	1.9
	L24906	June–July 1985	Single	First	4.0	0.49	

1933 and 1948 leveling) and postseismic (1983 to 1984) surveys are described by Stein and Barrientos (1985a, b). In this study, we use the 1933 to 1948 preseismic surveys and new postseismic leveling data acquired during July 1985. This data set consists of two lines: line 1 reoccupies the 1984 survey oriented normal to the fault, and line 2 (squares on Figure 3) runs parallel to the main fault trace at an average distance of 5 to 6 km on the downthrown block. Line 2 imposes stronger restrictions on the northern extension of the rupture surface than was available to Stein and Barrientos (1985b) and Ward and Barrientos (1986), and also bounds the slip on the en-echelon northern segment of the fault. The survey specification and standards of the 1933 to 1948 and the 1985 surveys are shown in Table 3. The postseismic survey includes 20 months of deformation that followed the earthquake. Stein and Barrientos (1985a) have shown that the 1983 to 1984 postseismic slip is 2 per cent of the coseismic slip; thus, the slip that we determined using the 1985 leveling is probably 2 to 5 per cent larger than the coseismic value. Since our intent is to discover the subsurface fault geometry, the inclusion of some postseismic (1983 to 1985) slip is incidental.

The rms signal is 463 mm and the rms pure error 12 mm. The rms signal to noise ratio is 38.

Fault scarp measurements. The total length of the surface rupture associated with this earthquake is about 36 km. The maximum vertical displacement reaches 2.7 m, with about 17 per cent of the slip left-lateral. The maximum surface throw along the northern fault segment is 1 m (Figure 3). The throw is generally less than 0.5 m on the en-echelon segment but reaches a maximum value of 1.6 m (Crone and Machete, 1984; Crone *et al.*, 1985).

PLANAR FAULT MODELS WITH UNIFORM SLIP

Single plane

We searched by trial and error for the parameters that best satisfy the data in the least-squares sense, inverting for the magnitude of the slip. In this procedure, only the leveling data was used, and we fixed the strike of the plane to be coincident with the trend of the fault trace. The best single plane is shown in Figure 13. The characteristics of this plane are: dip = 49°; slip = 2.2 m; width = 18 km; and fault length = 23 km. The total moment is 2.9×10^{19} N-m (for $\mu = 3.23 \times 10^{10}$ Pa) and the static stress drop is 3 MPa (30 bars), using Kanamori and Anderson's (1975) formula for stress drop of an infinitely long dip-slip fault. These values agree with those previously estimated by Stein and Barrientos (1985a, b). The rms misfit is 39 mm, four times the rms pure error.

Two planes

The misfit in line 2 suggests that a more complex model would improve the fit. We selected the position and dimensions of a second plane based upon the results

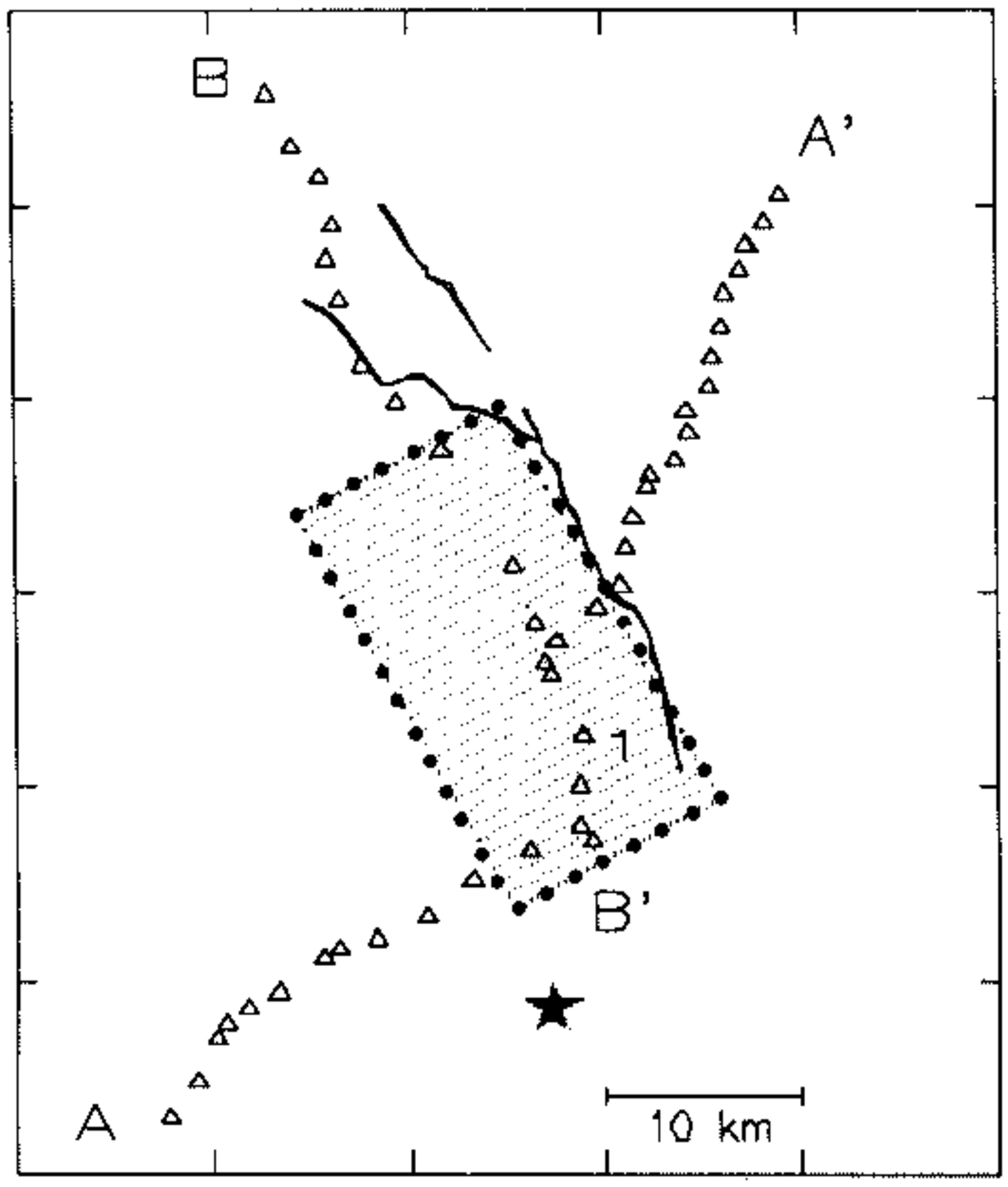

BORAH PEAK
Single Plane
Length : 23 km
Width : 18 km
Dip : 49°
Strike : 152°
x : 113°48 12 W
y : 44°04 08 N
Burial Depth : 0.0 km
Slip : 2.2 m
RMS misfit= 39.7 mm

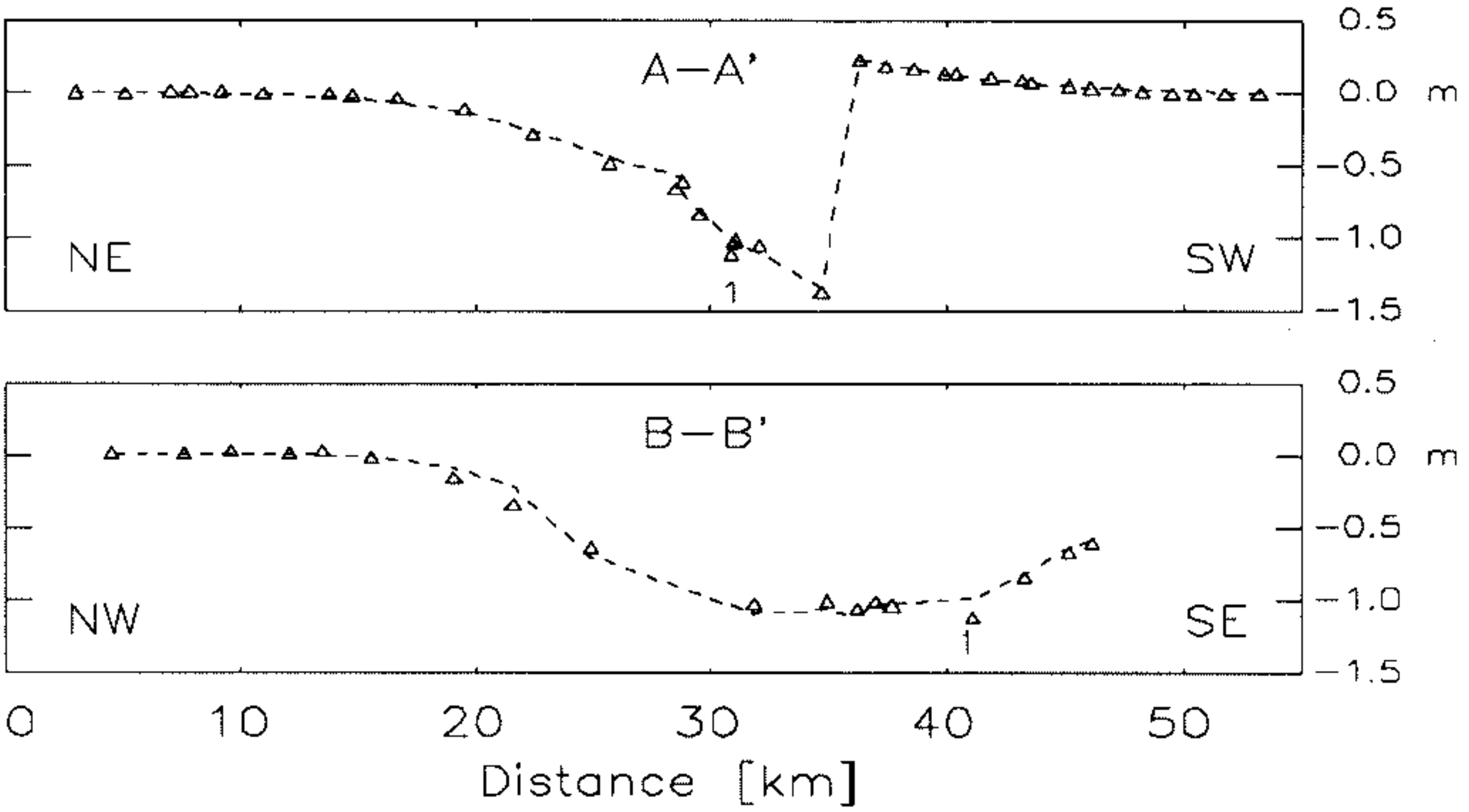

FIG. 13. Best single-plane model for Borah Peak. The *top box* shows the data distribution and the surface projection of the fault plane. Observations (solid) and predicted elevation change (dashed) along the lines A-A′ and B-B′ are shown in the *lower boxes*.

of Ward and Barrientos (1986), who found a thin segment (~10 km long by ~5 km width) with a maximum slip of 2 m. We varied the dimensions of both planes, but fixed the strike, dip slip angle (rake), and depth of burial to minimize the added degrees of freedom.

The best two-plane uniform slip model is shown in Figure 14. This model consists of two faults dipping 49°SW. The main plane is 18 × 18 km with 2.1 m of slip and a second 8 × 8 km plane with 1.4 m of slip located along strike northwestward of the main plane. The sum square of errors dropped from 0.062 to 0.029 m^2 when 6

degrees of freedom were added to define the northern fault segment. The F ratio is 3.3, significant at the 99 per cent confidence level. The inclusion of the second plane improves the correspondence between observed and predicted surface scarp offsets shown in Figure 10b (the solid line represents one uniform slip plane and the dashed line represents two planes). The rms misfit is 30 mm, 2.5 times the rms pure error. No further planes are required to fit the data, which indicates that slip on the northwestern en-echelon fault trace was surficial. Agreement of the model plane with focal mechanism of the main shock (Doser and Smith, 1985; Barrientos *et al.*, 1985) and aftershock locations (Richins *et al.*, 1985) can be seen in Figure 15.

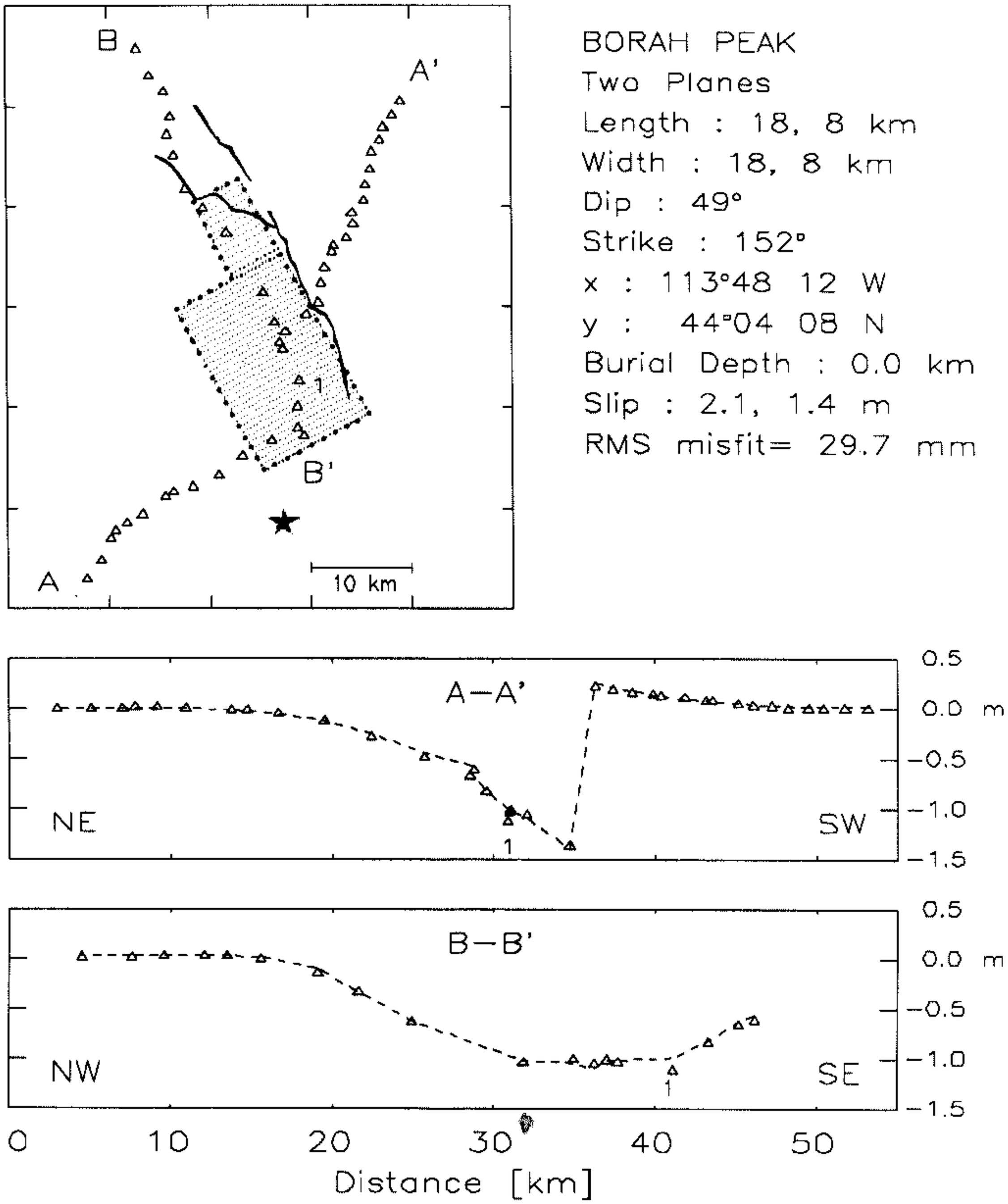

FIG. 14. Same as Figure 13 for the best two-plane model. This model produces a significantly better fit than the single-plane model, particularly toward the northern end of line B-B′.

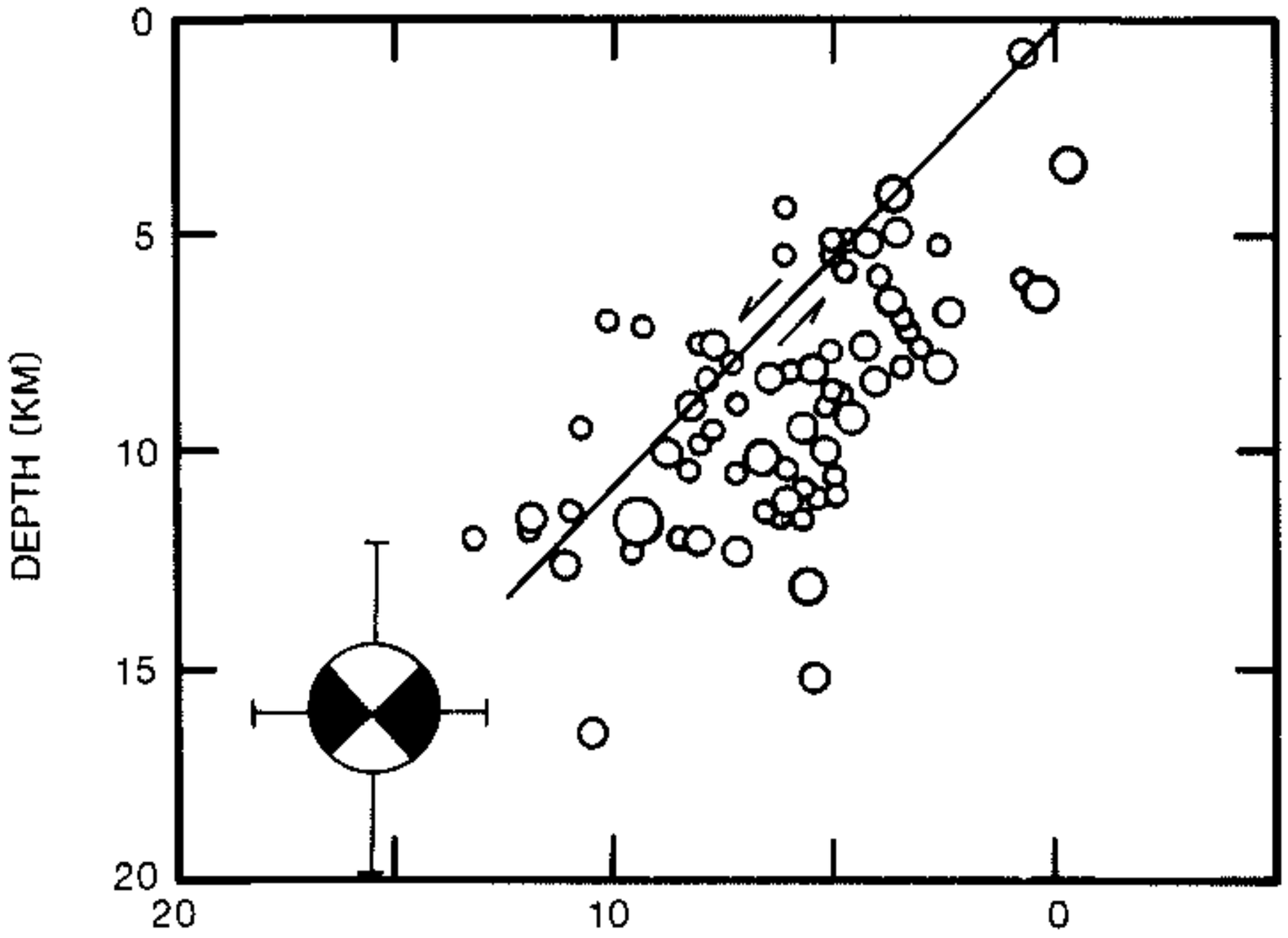

FIG. 15. Borah Peak coseismic model with main shock and aftershocks from Richins *et al.* (1985).

TABLE 4
COSEISMIC MODEL PARAMETERS

Earthquake	Plane No.	M_w Moment Magnitude	M_0 ($\times 10^{19}$ N-m)	$\Delta\sigma$ (MPa)	Slip (m)	Km				Listric Fault Shape
						Width	Length	Depth	Dip	
1959 Hebgen Lake, MT	1	7.1*	5.4	18	7.0–8.2	9–16	15–25	7–12	45°	Not demanded
	2	7.1*	6.8	11	6.5–7.8	11–18	15–25	9–14	50°	Not permitted
1983 Borah Peak, ID	1	6.9	2.5	2.2	2.1	18	18	14	49°	Not permitted
	2				1.4	8	8	6	49°	Not permitted

* Combined moment magnitude is 7.3.

Listric faults

Inversion for curvature was followed to determine whether the Lost River fault is listric at Borah Peak. Unlike the case for the Hebgen Lake event, the fit was degraded for any nonplanar combination of b_1 and b_2. Thus, neither listric nor antilistric faults are permitted by the data. This result confirms previous geodetic studies performed by Stein and Barrientos (1985b) and Ward and Barrientos (1986) with a smaller set of leveling data.

DISCUSSION

Given the different tectonic environments of Hebgen Lake and Borah Peak earthquakes, the geometric features common to both events are more important than their differences (Table 4). Both earthquakes occurred on nearly planar high-angle normal faults dipping 45° to 50°. Both earthquakes had slip extending to a depth of about 10 to 15 km. Neither of the events permits significant amounts of listric curvature of the faults at depth. The two planes associated with the Hebgen

Lake event and one with the Borah Peak earthquake also share similar moment-magnitudes (M = 7.1, 7.1, and 6.9). These features may typify large earthquakes in the Basin and Range Province. Larger event magnitudes are possible if more than 2 to 3 faults or fault segments rupture at once.

The fault-plane solutions and nucleation depths for the Hebgen Lake sequence derived from teleseismic long-period seismograms agree well with the coseismic model derived from geodetic observations, although there is some discordance in the strike of the Hebgen fault. The body wave solution is 110°E (Ryall, 1962; Doser, 1985), and we obtain an average value for the two planes of 132°E. The fault planes modeled for both earthquakes also coincide with aftershocks. In the Hebgen Lake region, the coseismic faults become more shallow toward the Yellowstone magma body, a feature that is shared by the seismicity of the region (Fournier and Pitt, 1985).

The most striking differences between the Hebgen Lake and Borah Peak earthquakes are the much greater slip (7.5 m versus 2 m), static stress drop (17 and 14 MPa versus 3 MPa), and the greater complexity of the Hebgen Lake earthquake. The seismically determined static stress drops are 9.7 MPa for the Hebgen Lake sequence (Doser, 1985) and 1.7 MPa for the Borah Peak event (Boatwright and Choy, 1986). From seismic records, the Borah Peak event appears as a simple unilateral rupture, whereas Hebgen Lake shows two events separated by 5 sec. The first subevent in the Hebgen Lake sequence, however, is so small ($M_0 = 3 \times 10^{18}$ N-m, stress drop = 1.8 MPa) that slip on both planes must be contained in the second subevent ($M_0 = 1 \times 10^{20}$ N-m).

Several investigators have proposed that low-angle faults are active at depths of 2 to 10 km in the Basin and Range (Wernicke, 1981; Smith and Bruhn, 1984). Geodetic modeling argues against shallow slip on listric faults at Borah Peak and Hebgen Lake. Stein and Barrientos (1985) concluded that slip did not occur on the preexisting White Knob low-angle thrust fault close to the Lost River fault. In the case of Hebgen Lake, the surface trace of the normal fault closely follows the Laramide thrust faults. The trace of the Red Canyon fault and the preexisting thrust both lie in a massive limestone or follow a contact between the limestone and thinly bedded shale. The trace of the Hebgen fault closely parallels a thrust fault in the limestone. This suggests that the limestone is the weaker element in the Laramide structure. Experimental evidence suggests that the strength of limestone diminishes more rapidly with depth than do silicate rocks (Olsson, 1974). Both the formerly active thrust faults and the currently active normal faults appear to have exploited the lower strength of the limestone bed within the sedimentary rocks. Neither fault can be traced beyond the limestone surface outcrop, although significant normal slip is modeled at depth in crystalline rocks at the ends of the fault. The surface association and the fault dips obtained from geodetic and body wave modeling imply that if normal slip occurred at depth on reactivated thrust sheets, the thrusts must dip about 50° and that these are not detachment or ramp features.

The two-plane geodetic model at Hebgen Lake does not satisfy two observations: the uplift centered on the bench marks 3 to 6 km north of Henrys Lake (Figure 2), and the 0.3 to 0.6 m subsidence of the north shore of Cliff Lake with respect to its southern end (see Figure 2). Reilinger *et al.* (1977) interpreted the former as an anomalous uplift in the broad doming of the region. The Cliff Lake tilt was based on casual observations (Myers and Hamilton, 1964, p. 78). Neither observation can be explained without localized sources. An aftershock, $M \approx 6.0$, occurred near Cliff

Lake about 48 hr after the main shock (Doser, 1985). The coseismic deformation associated with this event could be partly responsible for the observed subsidence.

Despite similar fault-plane area, the Hebgen Lake earthquake is much larger than the Borah Peak shock. Whereas the static stress drop for Borah Peak (~2 MPa) is typical of normal faulting events (Doser and Smith, 1985), and the 2-m surface slip is similar to the prehistoric rupture of this segment of the Lost River fault as well as other events on well-studied normal faults, such as the Wasatch (Schwartz and Coppersmith, 1984), rupture on the Red Canyon fault yields a stress drop an order of magnitude larger. Scant evidence from the height of the Holocene-Pleistocene fault scarps of the Red Canyon fault (Meyers and Hamilton, 1964, p. 65; Wallace, 1980) suggests that prehistoric rupture of the Hebgen Lake faults had a surface slip similar to the 1959 event.

It is possible that the higher stress required to break largely intact rock at the ends of the extending and coalescing faults results in a larger stress drop than for a central segment of a long, well-established fault. Laboratory evidence shows that larger stress drops accompany fracture of intact samples (Byerly, 1967; Summers and Byerly, 1977). The model faults extend well beyond mapped fault trace (Figures 9 and 11), which lends some support for this hypothesis. It is likely that the stress required to coalesce small fractures into one fault is less than that needed to break unfractured rocks, but perhaps it is still greater than that required to cause slip along straighter faults. There is, however, little evidence to suggest that large earthquakes on older straight faults have lower stress drops than young short faults.

Conclusions

Geodetic analysis of the Borah Peak static deformation field reveals, in agreement with previous studies, that the observations can be satisfactorily explained by one planar, nonlistric, uniform-slip source on a segment of the Lost River fault. This plane, 26 km long, dips 49° and decreases its width from 18 to 8 km and its slip from 2.1 to 1.4 m in the northwestern segment of the rupture.

Similar analyses in the Hebgen Lake region reveal a more complex source. The source consists of at least two en-echelon planes that coincide with new scarps along Hebgen and Red Canyon faults. Both planes are 15 to 25 km long, dip 45° to 50°, with 7.0 to 7.8 m of slip. The Red Canyon fault may be slightly listric, but the Hebgen Lake fault must be planar. It is particularly interesting that this normal fault does not become listric at depth even though there is a Laramide thrust fault in proximity. If normal slip occurred at depth on the reactivated thrust fault, the thrust fault must dip at about 50°.

West of Hebgen Lake, coseismic slip in 1959 of the Madison Range normal fault could not have exceeded 1 m ($M_0 = 4.6 \times 10^{18}$ N-m). Our model does not permit more than 1 m of slip along the Madison Range fault and is consistent with the absence of deep slip. Thus, the "dual-basin" hypothesis is inconsistent with our results.

The geodetic models for both events are consistent with depth and focal mechanism of the main event and aftershock locations. In the case of Hebgen Lake, the strike of the faults is slightly discordant with that predicted by the seismic fault plane solution.

Acknowledgments

We would like to thank Mitch Pitt, for providing his excellent record of Yellowstone seismicity. Robert Christiansen, Warren Hamilton, Bob Smith, and Irving Witkind taught us much about the

Quaternary geology of Hebgen Lake. Gary Perasso located vital Hebgen Lake field books from the U.S. Geological Survey archives. Bob Martine and Emery Balazs guided the skilled NGS releveling effort at Borah Peak, and Dan Dzurisin performed the 1986 Hebgen Lake leveling. Diane Doser and Walter Arabasz reviewed this paper. This work has been partially funded by U.S. Geological Survey Contracts 14-08-0001-G1157 and 14-08-0001-G1383.

REFERENCES

Allmendinger, R. W., J. W. Sharp, D. von Tish, L. Serpa, L. Brown, S. Kaufman, and J. Oliver (1983). Cenozoic and Mesozoic structure of the Eastern Basin and Range Province, Utah, from COCORP seismic-reflection profile data, *Geology* **11,** 532–536.

Barrientos, S. E., S. N. Ward, J. González-Ruiz, and R. S. Stein (1985). Inversion for Moment as a function of depth from geodetic observations and long period body waves of the 1983 Borah Peak, Idaho, earthquake, Workshop XXVIII on the Borah Peak Earthquake, *U.S. Geol. Surv., Open-File Rept. 85-290*, 485–518.

Boatwright, J. and G. L. Choy (1986). Teleseismic estimates of the energy radiated by shallow earthquakes, *J. Geophys. Res.* **91,** 2095–2112.

Bomford, G. (1971). *Geodesy*, Oxford University Press, London, England.

Bond, J. G. (1978). Geologic map of Idaho, Idaho Bureau of Mines and Geology, Moscow, USSR.

Chi, S. C., R. E. Reilinger, L. D. Brown, and J. E. Oliver (1980). Leveling circuits and crustal movements, *J. Geophys. Res.* **85,** 1469–1474.

Chinnery, M. A. (1961). The deformation of the ground around surface faults, *Bull. Seism. Soc. Am.* **51,** 355–372.

Christiansen, R. L. (1986). The Quaternary and Pliocene Yellowstone Plateau volcanic field of Wyoming, Idaho, and Montana, *U.S. Geol. Surv. Profess. Paper 729-G*, 221 pp.

Crone, A. J. and M. N. Machete (1984). Surface faulting accompanying the Borah Peak earthquake, central Idaho, *Geology* **12,** 664–667.

Crone, A. J., M. N. Machete, M. G. Bonilla, J. J. Lienkaemper, K. L. Pierce, W. E. Scott, and R. C. Bucknam (1985). Characteristics of surface faulting accompanying the Borah Peak earthquake, central Idaho, Workshop XXVIII on the Borah Peak Earthquake, *U.S. Geol. Surv., Open-File Rept. 85-290*, 43–58.

Doser, D. I. (1985). Source parameters and faulting of the 1959 Hebgen Lake, Montana earthquake sequence, *J. Geophys. Res.* **90,** 4537–4555.

Doser, D. I. and R. B. Smith (1985). Source parameters of the October 28, 1983 Borah Peak, Idaho earthquake from body wave analysis, *Bull. Seism. Soc. Am.* **75,** 1041–1051.

Eaton, G. P., R. L. Christiansen, H. M. Iyer, A. M. Pitt, D. R. Mabey, H. R. Blank, Jr., I. Zietz, and M. E. Gettings (1975). Magma beneath Yellowstone National Park, *Science* **188,** 787–796.

Fraser, G. D., I. J. Witkind, and W. H. Nelson (1964). A geological interpretation of the epicentral area—The dual-Basin concept, *U.S. Geol. Surv. Profess. Paper 435*, 99–106.

Fournier, R. O. and A. M. Pitt (1985). The Yellowstone magmatic hydrothermal system, U.S.A., in *Geothermal Resources Council*, International Symposium on Geothermal Energy, International Volume, Claudia Stone, Editor, Geothermal Resources Council, Davis, California, 319–327.

Hanks, T. C. and H. Kanamori (1979). A moment magnitude scale, *J. Geophys. Res.* **84,** 2348–2350.

Holdhal, S. R. (1981). A model of temperature stratification for correction of leveling refraction, *Bull. Geod.* **55,** 231–249.

Kanamori, H. and D. L. Anderson (1975). Theoretical basis of some empirical relations in seismology, *Bull. Seism. Soc. Am.* **65,** 1073–1095.

Langbein, J., A. McGarr, M. J. S. Johnston, and P. W. Harsh (1983). Geodetic measurements of postseismic crustal deformation following the 1979 Imperial Valley earthquake, California, *Bull. Seism. Soc. Am.* **73,** 1203–1224.

Mathieson, E. L. (1983). Late Quaternary activity of the Madison Range Fault along its 1959 rupture trace, Madison County, Montana, *Master's Thesis*, Stanford University, Stanford, California.

Myers, W. B. and W. Hamilton (1964). Deformation accompanying the Hebgen Lake earthquake of August 17, 1959, *U.S. Geol. Surv. Profess. Paper 435*, 55–98.

Nash, D. B. (1984). Morphologic dating of fluvial terrace scarps and fault scarps near West Yellowstone, Montana, *Geol. Soc. Am. Bull.* **95,** 1413–1424.

Okada, Y. (1985). Surface deformation due to shear and tensile faults in a half-space, *Bull. Seism. Soc. Am.* **75,** 1135–1154.

Olsson, W. A. (1975). Effects of temperature, pressure and displacement rate on the frictional characteristics of a limestone, *J. Rock Mech., Mat. Sci. Geomech.* **11,** 267–278.

Pitt, A. M. (1987). Catalog of earthquakes in the Yellowstone Park-Hebgen Lake region from 1973 to 1981, *U.S. Geol. Surv., Open-File Rept.* (in press).

Reilinger, R. E., G. P. Citron, and L. D. Brown (1977). Recent vertical crustal movements from precise leveling data in southwestern Montana, western Yellowstone National Park, and the Snake River plain, *J. Geophys. Res.* **82,** 5349–5959.

Reilinger, R. E. (1985). Vertical movements associated with the 1959, $M = 7.1$ Hebgen Lake Montana earthquake, Workshop XXVIII on the Borah Peak Earthquake, *U.S. Geol. Surv., Open-File Rept. 85-290*, 510–530.

Reilinger, R. E. (1986). Evidence for postseismic viscoelastic relaxation following the 1959 $M = 7.5$ Hebgen Lake, Montana, earthquake, *J. Geophys. Res.* **91,** 9488–9494.

Richins, W. D., R. B. Smith, C. J. Langer, J. E. Zollweg, J. T. King, and J. C. Pechmann (1985). The 1983 Borah Peak, Idaho earthquake: relationship of aftershocks to mainshock, surface faulting, and regional tectonics, Workshop XXVIII on the Borah Peak Earthquake, *U.S. Geol. Surv., Open-File Rept. 85-290*, 285–310.

Romney, C. (1957). Seismic waves from the Dixie Valley-Fairview Peak earthquakes, *Bull. Seism. Soc. Am.* **47,** 301–319.

Ryall, A. (1962). The Hebgen Lake, Montana, earthquake of August 18, 1959: *P* waves, *Bull. Seism. Soc. Am.* **52,** 235–271.

Savage, J. C. and L. M. Hastie (1966). Surface deformation associated with dip-slip faulting, *J. Geophys. Res.* **71,** 4897–4904.

Savage, J. C. and L. M. Hastie (1969). A dislocation model for the Fairview Peak, Nevada, earthquake, *Bull. Seism. Soc. Am.* **59,** 1937–1948.

Savage, J. C., M. Lisowski, and W. H. Prescott (1985). Strain accumulation in the Rocky Mountain States, *J. Geophys. Res.* **90,** 10310–10320.

Scott, W. E., K. L. Pierce, and M. H. Hait, Jr. (1985). Quaternary tectonic setting of the 1983 Borah Peak earthquake, Central Idaho, *Bull. Seism. Soc. Am.* **75,** 1053–1066.

Smith, R. B. and R. L. Bruhn (1984). Intraplate extensional tectonics of the eastern Basin-Range: inferences on structural style from seismic reflection data, regional tectonics, and thermal-mechanical models of brittle-ductile deformation, *J. Geophys. Res.* **89,** 5733–5762.

Smith, R. B. and R. L. Christiansen (1980). Yellowstone National Park as window on the earth's interior, *Sci. Am.* **242,** 104–117.

Stein, R. S. (1981). Discrimination of tectonic displacement from slope-dependent errors in geodetic leveling from southern California, 1953–1979, in *Earthquake Prediction—An International Review,* Maurice Ewing series, vol. 4, D. W. Simpson and P. G. Richards, Editors, American Geophysical Union, Washington, D.C., 441–456.

Stein, R. S. and S. Barrientos (1985a). The 1983 Borah Peak, Idaho, earthquake: geodetic evidence for deep rupture on a planar fault, Workshop XXVIII on the Borah Peak Earthquake, *U.S. Geol. Surv., Open-File Rept. 85-290*, 459–484.

Stein, R. S. and S. Barrientos (1985b). High-angle normal faulting in the intermountain seismic belt: geodetic investigation of the 1983 Borah Peak, Idaho, earthquake, *J. Geophys. Res.* **90,** 11355–11366.

Stein, R. S., C. T. Whalen, S. R. Holdahl, W. E. Strange, and W. Thatcher (1986). Saugus-Palmdale, California: Field test for refraction error in historical leveling surveys, *J. Geophys. Res.* **91** (in press).

U.S. Geological Survey (1964). The Hebgen Lake, Montana earthquake of August 17, 1959, *U.S. Geol. Surv. Profess. Paper 435.*

U.S. Geological Survey (1972). Geologic Map of Yellowstone National Park, *U.S. Geol. Surv. Misc. Investigations Map I-711.*

Wallace, R. E. (1980). Degradation of the Hebgen Lake fault scarp of 1959, *Geology* **8,** 225–229.

Wallace, R. E. (1984a). Fault scarps formed during the earthquake of October 2, 1915, in Pleasant Valley, Nevada, and some tectonic implications, *U.S. Geol. Surv. Profess. Paper 1274-A.*

Ward, S. N. and S. E. Barrientos (1986). An inversion for slip distribution and fault shape from geodetic observations of the 1983, Borah Peak, Idaho, earthquake, *J. Geophys. Res.* **91,** 4909–4919.

Wernicke, B. (1981). Low-angle normal faults in the Basin and Range province: Nappe tectonics in an extending orogen, *Nature* **291,** 645–648.

Witkind, I. J. (1964). Reactivated faults North of Hebgen Lake, *U.S. Geol. Surv. Profess. Paper 435*, 37–50.

Witkind, I. J. (1975a). Preliminary map showing known and suspected active faults in Wyoming, *U.S. Geol. Surv., Open-File Rept. 75-279*, 36 pp.

Witkind, I. J. (1975b). Preliminary map showing known and suspected active faults in Western Montana, *U.S. Geol. Surv., Open-File Rept. 75-285*, 36 pp.

Witkind, I. J. (1975c). Preliminary map showing known and suspected active faults in Idaho, *U.S. Geol.*

Surv., Open-File Rept. 75-278, 71 pp.
Witkind, I. J., W. B. Myers, J. H. Hadley, W. Hamilton, and G. D. Fraser (1962). Geologic features of the earthquake at Hebgen Lake, Montana, August 17, 1959, *Bull. Seism. Soc. Am.* **52**, 163–180.

C. F. RICHTER SEISMOLOGICAL LABORATORY
EARTH SCIENCES BOARD
UNIVERSITY OF CALIFORNIA, SANTA CRUZ
SANTA CRUZ, CALIFORNIA 95064
CONTRIBUTION NO. 37 (S.E.B., S.N.W.)

U.S. GEOLOGICAL SURVEY
345 MIDDLEFIELD ROAD
MENLO PARK, CALIFORNIA 94025 (R.S.S.)

Manuscript received 4 July 1986

The present address of Sergio E. Barrientos is: Departamento de Geofísica, Universidad de Chile, Casilla 2777, Santiago, Chile.

ERRATA

Bulletin of the Seismological Society of America
Vol. 77, June 1987, pp. 784–808

COMPARISON OF THE 1959 HEBGEN LAKE, MONTANA, AND THE 1983 BORAH PEAK, IDAHO, EARTHQUAKES FROM GEODETIC OBSERVATIONS

By Sergio E. Barrientos, Ross S. Stein, and Steven N. Ward

We regret that the geographical coordinates given in Barrientos *et al.* (1987) for the model faults in Figures 8, 9, and 12 were incorrect. The correct coordinates for the mid-point of the upper edge (or top) of the model fault, projected vertically to the ground surface, are as follows:

Hebgen Lake earthquake, best single-fault planar model (Fig. 8):
latitude: 44°49.7′ longitude: 111°15.0′

Hebgen Lake earthquake, best two-fault planar model (Fig. 9):
Plane 1: latitude: 44°49.6′ longitude: 111°12.0′
Plane 2: latitude: 44°51.6′ longitude: 111°18.7′

Hebgen Lake earthquake, best listric two-fault planar model (Fig. 12):
Plane 1: latitude: 44°49.6′ longitude: 111°12.0′
Plane 2: latitude: 44°51.6′ longitude: 111°18.7′

In addition, the definition for the degrees of freedom in the equation for the *F*-statistic on p. 794 are incorrect. The parameter $\nu_1 = N - f_1 - 1$, and $\nu_2 = N - f_2 - 1$. All other source parameters and equations given in the text, tables, and figures are correct. We thank Sanford R. Holdahl of the National Geodetic Survey for bringing this error to our attention.